Title

SPORA, a new silver phosphate precipitation protocol for oxygen isotope analysis of small, organic-rich bioapatite samples

Authors

Conte, Gabriele Larocca

Lopes, Lauren E

Mine, Aric H

et al.

Publication Date

2024-04-01

DOI

10.1016/j.chemgeo.2024.122000

Peer reviewed

Chemical Geology 651 (2024) 122000

Contents lists available at ScienceDirect

Chemical Geology

journal homepage: www.elsevier.com/locate/chemgeo

SPORA, a new silver phosphate precipitation protocol for oxygen isotope analysis of small, organic-rich bioapatite samples

Gabriele Larocca Conte [a,*], Lauren E. Lopes [a], Aric H. Mine [b], Robin B. Trayler [a], Sora L. Kim [a]

[a] Department of Life & Environmental Sciences, University of California Merced, 5200 Lake Rd, Merced, CA 95343, United States of America
[b] Department of Earth and Environmental Sciences, California State University, Fresno, 5241 N Maple Ave, Fresno, CA 93740, United States of America

ARTICLE INFO

Editor: Dr. Oleg Pokrovsky

Keywords:
Silver phosphate
Oxygen isotopes
Paleoecology
Archeology
Paleoclimate
Anion exchange resin

ABSTRACT

Isotopic analysis of phosphate oxygen from bones and teeth ($^{18}O_p/^{16}O_p$, $\delta^{18}O_p$) is a common tool used to investigate modern and ancient ecosystems and their climate. However, existing methods have expanded to use pretreatments for organic removal, require large sample sizes, or require extended precipitation timing. All together, these factors could affect accuracy and precision of $\delta^{18}O_p$ measurement by promoting the formation of oxygen-bearing or nitrogen-rich contaminants. However, the nature and occurrence of contamination are not fully explored. Here we sought to develop a method of silver phosphate precipitation that tests the effect of different sample treatments and reduced sample sizes while preserving sample isotopic composition.

Our protocol (SPORA) precipitates Ag_3PO_4 crystals from ~1.5 mg of starting material while purifying phosphate from contaminants, like nitrogen or carbonate. Isolation and purification of phosphate are achieved with an anion exchange resin, followed by precipitation of silver phosphate using an updated silver ammine solution that targets small amounts of phosphate in solution. We used a variety of phosphate oxygen reference materials and biogenic apatite materials, such as modern and fossil specimens with varying collagen content, to test the SPORA protocol and its effects on the resultant phosphate oxygen isotopic composition. Results were then compared to those from another published silver phosphate precipitation method (i.e., Rapid University of Chicago Dilute, Rapid UC). Overall, $\delta^{18}O_p$ values of standards and biogenic apatites were similar between protocols ($R^2 = 0.99$, $p << 0.05$). In addition to isotope composition comparisons, UV–Vis spectroscopy and Fourier Transform Infrared (FTIR) analyses discerned phosphate recovery and material composition of crystals precipitated via different protocols, respectively. We found that the resin *i*) may retain ~10% of phosphate with no isotopic effects and *ii*) the SPORA protocol produces Ag_3PO_4 with more accurate $\delta^{18}O_p$ measurements by preventing the formation of contaminant oxygen phases, silver oxide (Ag_2O) and silver carbonate (Ag_2CO_3), that confound the phosphate oxygen isotope composition.

The SPORA Ag_3PO_4 precipitation procedure overcomes analytical limitations such as sample size and collagen contamination, conditions that other procedures for $\delta^{18}O_p$ analysis cannot address simultaneously. The SPORA protocol can be used on a large array of bioapatite materials for paleoecological, paleoclimatic, and archeological applications, while reducing the required sample size and ensuring pure Ag_3PO_4 for isotopic analysis.

1. Introduction

Skeletal materials and their phosphate oxygen isotope composition ($^{18}O/^{16}O$, $\delta^{18}O$) provide invaluable environmental records to investigate climatic variability (e.g., temperature, salinity, aridity) and ecology of humans and animals across modern and geological time scales (e.g., movements, breastfeeding, and weaning practices) (Kim et al. 2014, 2020; Kirsanow et al., 2008; Kocsis et al., 2014; Kohn and Cerling, 2003; McMahon et al., 2013; Newsome et al., 2010; Pearson et al., 2009; Pederzani and Britton, 2019; Tsutaya and Yoneda, 2015; Vennemann and Hegner, 1998; Zacke et al., 2009). These applications rely on the body temperature-dependent fractionation of oxygen isotopes between ingested water and mineral phases, primarily composed of biogenic apatite ($Ca_{10}(PO_4, xCO_3)_{6-x}(OH, F, yCO_3)_{2-y}$) (Dorozhkin, 2009; Enax et al., 2012; Lübke et al., 2015). Phosphate oxygen ($\delta^{18}O_p$) is often preferred over carbonate (CO_3^{2-}) $\delta^{18}O$ values given its stability against diagenetic alteration (Koch et al., 1997; Kohn et al., 1999; Kolodny et al., 1983; Shemesh et al., 1983; Stephan, 2000; Zazzo et al., 2004).

* Corresponding author.
E-mail address: glaroccaconte@ucmerced.edu (G. Larocca Conte).

https://doi.org/10.1016/j.chemgeo.2024.122000
Received 31 May 2023; Received in revised form 12 February 2024; Accepted 21 February 2024
Available online 28 February 2024

The analysis of stable oxygen isotope compositions ($^{18}O_p/^{16}O_p$, $\delta^{18}O_p$) from vertebrate skeletal remains requires the isolation of the phosphate component (i.e., PO_4^{3-} ion) after dissolving bioapatite in an acid solution and precipitating it into a salt that serves as an analytical substrate. Silver phosphate (Ag_3PO_4) is considered a suitable analyte given its non-hygroscopic nature, preventing adsorption of ambient water and incorporation of oxygen derived from moisture. Silver phosphate crystals are commonly measured via high temperature reduction (i.e., HTR) of Ag_3PO_4 to carbon monoxide (CO) methods coupled to an Isotope Ratio Mass Spectrometer (IRMS) (Fourel et al., 2011; Lécuyer et al., 2007; Vennemann et al., 2002). Current Ag_3PO_4 precipitation protocols for IRMS analysis differ in terms of the starting amount of apatite material, treatments to remove organics (e.g., pre-treatments via NaOCl vs anion exchange purification before Ag_3PO_4 precipitation), phosphate dissolution (e.g., HF, HNO_3, or both) and rate of crystal precipitation (e.g., rapid (~10 min) or slow (~13 h)) (Crowson et al., 1991; Dettman et al., 2001; Firsching, 1961; Griffin et al., 2015; Lécuyer et al., 1998; Lécuyer et al., 1993; Mine et al., 2017; O'Neil et al., 1994; Pederzani et al., 2020; Quinton et al., 2016; Royer et al., 2013; Shabaga et al., 2018; Stephan, 2000; Sun et al., 2016; Tütken et al., 2006; Wiedemann-Bidlack et al., 2008). These techniques result in silver phosphate for $\delta^{18}O_p$ values, but may not be ideal for variably organic-rich biogenic apatite, small sample sizes, and starting material of varying burial history. Finally, many previous silver phosphate methodologies do not directly test or quantify the possibility of contamination in silver phosphate crystals.

Sample size, contaminant inclusions, and the form of apatite (i.e., bone, dentin, enamel, enameloid) may affect the oxygen isotope composition of the precipitated Ag_3PO_4. Protocols often recommend 4 to 10 mg of drilled starting materials (e.g., Pederzani et al., 2020; Tütken et al., 2006; Shabaga et al., 2018), which is a problem when dealing with smaller specimens, such as teeth. Small tooth specimens (i.e., <2 cm tall) often necessitate crushing, yielding a mixture of enamel (or enameloid in sharks) and dentin. Like bone samples, dentin, contains a high collagen content (up to ~20%wt. against <4%wt. in enamel or enameloid) (Koch et al., 1997; Lee-Thorp, 2002; Lee-Thorp and van der Merwe, 1991; LeGeros, 1981), which, if not removed, releases nitrogen-rich compounds that could contaminate Ag_3PO_4 crystals and leads to inaccurate $\delta^{18}O_p$ values during IRMS analysis (Kornexl et al., 1999). Common collagen removal treatments require soaking powdered samples in sodium hypochlorite solution (NaOCl, "bleach") before bioapatite dissolution to minimize the coprecipitation of such nitrogen compounds during the precipitation of Ag_3PO_4 crystals (Lécuyer, 2004; Mine et al., 2017; O'Neil et al., 1994; Pederzani et al., 2020; Stephan, 2000; Vennemann et al., 2002; Wiedemann-Bidlack et al., 2008). However, NaOCl pre-treatment for Ag_3PO_4 protocols is discouraged due to unpredictable isotopic shifts (Grimes and Pellegrini, 2013; Pederzani et al., 2020). If nitrogen-rich organic compounds are not the cause of contamination, collagen breakdown after bleach pre-treatment could possibly promote carbonate contamination (Crowley and Wheatley, 2014; Pellegrini and Snoeck, 2016; Snoeck and Pellegrini, 2015), but its specific effect on Ag_3PO_4 isotopic fidelity has not been explored. Finally, extended reaction times to precipitate silver phosphate crystals (e.g., Griffin et al., 2015; Pederzani et al., 2020; Royer et al., 2013; Wiedemann-Bidlack et al., 2008) may lead to the incorporation of oxygen-bearing minerals (e.g., Ag_2CO_3 and/or silver oxide (Ag_2O)) and associated isotopic shifts. More rapid reaction times when precipitating Ag_3PO_4 crystals are desired to prevent contamination. Ideally, a silver phosphate precipitation method would require minimal bioapatite sample, isolate apatite phosphate despite the presence of contaminants, and limit the incorporation of these contaminants in silver phosphate crystals.

In addition, structural differences and burial processes determine the carbonate content in biological apatite materials. Bone and dentin have higher structural carbonate content (i.e. carbonate within the bioapatite crystal lattice structure) and porosity than enamel or enameloid (Lee-Thorp and van der Merwe, 1991; LeGeros, 1981). Exogenous compounds, such as natural asphalt or secondary carbonate minerals like calcite, often fill pore spaces of dentin and bone following the burial of skeletal remains (Fox-Dobbs et al., 2014; Fox-Dobbs et al., 2006; France et al., 2015; Fuller et al., 2014; Pederzani and Britton, 2019; Schwarcz and Schoeninger, 1991; Zazzo et al., 2004). Protocols for Ag_3PO_4 precipitation would ideally prevent carbonate contamination, which could be structural from inorganics or organic sources, including carbon dioxide outgassing during the apatite dissolution in acid mediums. The formation of silver carbonate (Ag_2CO_3) was recently identified as a possible major contaminant phase in the silver phosphate salt (Mine et al., 2017), and therefore the occurrence and contribution of all such carbonate contaminants in Ag_3PO_4 crystals needs to be assessed.

Here, we aimed to design a new precipitation protocol: the SPORA protocol (i.e., Silver Phosphate Oxygen Resin Analysis). This approach requires less starting material (~1.5 mg or less) and precipitates silver phosphate crystals following phosphate isolation via an anion exchange resin. Anion exchange resins were previously used to isolate phosphate from bioapatite and water (Colman, 2002; Colman et al., 2005; Crowson et al., 1991; Goldhammer et al., 2011; Goldhammer et al., 2010; Lécuyer et al., 1998; Pederzani et al., 2020; Royer et al., 2013), but the SPORA protocol is unique given its minimal starting material (~1.5 mg or less), exclusion of organic contaminants, and consistent phosphate oxygen isotope composition. We tested the SPORA protocol with respect to carbonate and nitrogen-rich samples, hypothesizing that the resin adsorbs phosphate while excluding contaminants and improving phosphate $\delta^{18}O$ values. We assessed silver phosphate recovery, composition, and purity within our method using Fourier-Transform Infrared (FTIR) and UV–Vis spectrophotometry analyses as complementary tools to quantify mineral composition and quality of silver phosphate crystals as well as phosphate yield, respectively.

2. Materials and methods

We compared our new silver phosphate protocol with the Rapid University of Chicago Dilute (i.e., Rapid UC) technique after Mine et al. (2017) because both procedures include two similar, fundamental steps: *i*) calcium fluoride (CaF_2) precipitation to isolate phosphate from the structural ions of apatite (e.g., Ca^{2+} and F^-) and *ii*) an instantaneous silver phosphate (Ag_3PO_4) precipitation using a silver ammine solution. The main difference between protocols is the organic matter removal step. SPORA uses an anion exchange resin (Bio-Rad AG™ 1-X8) (Bio-Rad Laboratories, 2000) to isolate phosphate ions from organic residuals between the CaF_2 precipitation and Ag_3PO_4 precipitation (Fig. 1).

We assess the SPORA protocol performance in terms of $\delta^{18}O$ accuracy, phosphate recovery, and contaminant exclusion. We tested the SPORA protocol on samples of varying nature, such as organic content and depositional settings. Data were processed using R Studio (RStudio Team, 2021). The complete dataset and R code scripts to elaborate on corrections and analysis are found in supplementary materials for transparency. A detailed description and a schematic diagram of the procedure are also part of the supplementary materials.

2.1. Sample descriptions

We used biogenic apatite specimens and commercially available inorganic reference materials to test the similarity in $\delta^{18}O_p$ values between protocols. Inorganic working reference materials included: NIST SRM 120c (Florida phosphate rock, National Institute of Standards and Technology), synthetic hydroxyapatite (Sigma Aldrich, CAS: 12167-74-7), and naturally occurring fluorapatite (Fisher Scientific, CAS: 1306-05-4). Enamel and enameloid powder (i.e., enamel and enameloid powder, <4%wt collagen) were drilled from (i) a modern goat tooth specimen, (ii) teeth of the functional file series of a modern, blue shark jaw, and (iii) two fossil sand tiger shark teeth (SM1 and SM2 specimens, Table 1). We used a mixture of enamel and dentin from the same tooth specimens

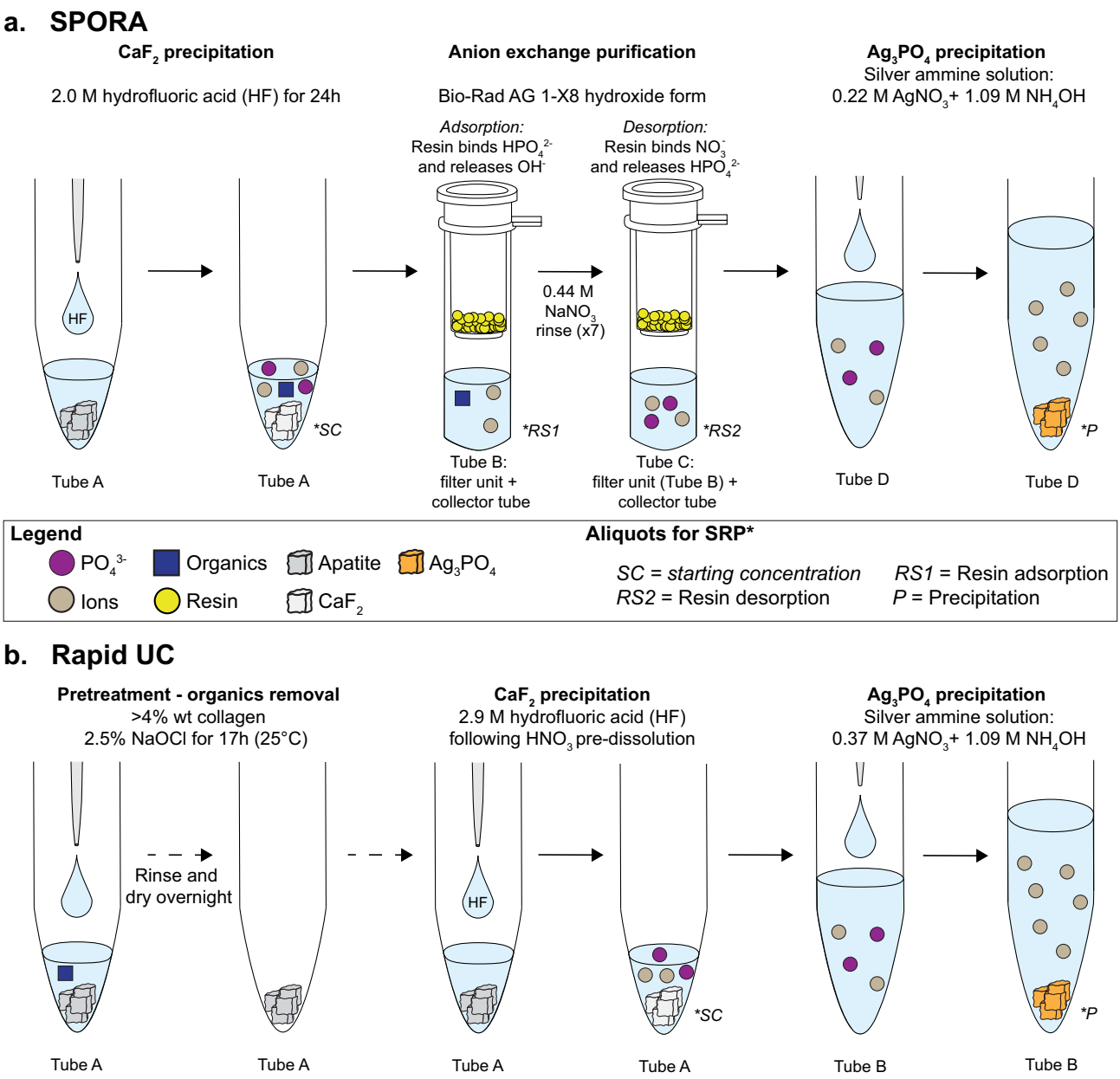

Fig. 1. A graphical overview of (a) SPORA and (b) Rapid UC protocols indicating similar steps in CaF_2 removal and Ag_3PO_4 precipitation as well as deviations, such as pretreatment and anion exchange purification. Dashed arrows indicate that the pretreatment step for Rapid UC method is not mandatory, but it is applied only when samples are of high organic content. Italicized abbreviations indicate where aliquots for SRP analysis were taken.

and bone samples (Table 1) to test the anion exchange resin on materials of different burial settings and with an expected high organic content (>4%wt collagen). A goat tooth was drilled on the occlusal surface of the second cusp to obtain the enameloid/dentin mixture and modern shark teeth were crushed. Bone specimens used for this study belong to a modern deer individual and two indeterminate, fossil mammal taxa, including a specimen from tar seep deposits (MM1; Table 1). Natural asphalt inclusions lead to inaccurate $\delta^{13}C$ and $\delta^{15}N$ values (Fox-Dobbs et al., 2006, 2014; Fuller et al., 2014), and therefore we believed that $\delta^{18}O_p$ measurements are no exception. We used the MM1 specimen to test whether the resin efficiently removes tar from samples. We dissolved the natural asphalt from the powdered bone by sonicating the powder in a toluene-methanol solution following Fuller et al. (2014) (MM1, bone (tar removed), Table 1; see **SM1** for a detailed description of the procedure) and compared results with those of the untreated powder.

Given the initial application of this method, we also specifically tested SPORA with modern and fossil shark teeth. We used a mixture of enameloid and dentin in shark teeth from the same specimen to test the anion exchange resin. We treated individual teeth of the modern shark as separate samples, except for "TOM_1" that includes a homogeneous mixture of enameloid powder from two clipped teeth (Table 1). Additionally, we prepared an enameloid/dentin mixture by ball-milling a mixture of shark teeth clipped from the same jaw (TOM_6; Table 1) to test the resin's application on materials with an expected high organic content (>4%wt collagen). Similarly, for each fossil shark tooth sample, we crushed a single chunk of the crown to obtain a mixture of dentin and enameloid of the same specimens.

We tested the features of inorganic or organic contaminant inclusions in silver phosphate crystals and their effect on $\delta^{18}O$ accuracy. We used a silver phosphate standard (Alfa Aesar; CAS: 7784-09-0) and mixed it with collagen from bovine achilles tendon (Sigma Aldrich; CAS:

Table 1
The SPORA protocol was tested on apatite materials of varying nature and organic content using small sample size (~ 1.5 mg). The table shows samples used, ID code assigned to samples, number of replicates, starting amount, and material types analyzed with SPORA and Rapid UC protocols, which was used to compare protocols' performance. The mass of the starting amount is calculated from the weight of each replicate per protocol and reported as mean ± 1σ.

Sample	ID	# Specimens	Material	# Replicates		Mass (mg; mean ± sd)	
				Rapid UC	SPORA	Rapid UC	SPORA
Fluorapatite	FA	1	Naturally occurring crystal	10	12	1.02 ± 0.04	1.07 ± 0.07
Fossil mammal indet (1)	MM1	1	Bone (tar not removed)	–	5	–	1.86 ± 0.11
			Bone (tar removed)	5	5	1.71 ± 0.15	1.81 ± 0.06
Fossil mammal indet (2)	MM2	1	Bone	5	5	1.76 ± 0.16	1.79 ± 0.15
Fossil shark	SM1	1	Enameloid	5	5	1.06 ± 0.02	1.13 ± 0.06
			Enameloid + dentin	5	5	1.71 ± 0.15	1.80 ± 0.14
Fossil shark	SM2	1	Enameloid	5	5	1.05 ± 0.04	1.17 ± 0.07
			Enameloid + dentin	5	5	1.76 ± 0.16	1.73 ± 0.14
Hydroxyapatite	HAP	1	Synthetic crystal	10	11	1.04 ± 0.05	1.10 ± 0.09
Modern deer	OV	1	Bone	5	5	1.97 ± 0.05	1.84 ± 0.09
Modern goat	CH	1	Enamel	10	5	1.14 ± 0.09	1.13 ± 0.04
			Enamel + dentin	5	5	1.77 ± 0.16	1.89 ± 0.14
Modern shark	TOM_1	2	Enameloid	1	1	1.08	1.25
			Enameloid + dentin	1	1	1.03	1.75
	TOM_2	1	Enameloid	1	1	1.12	1.25
			Enameloid + dentin	1	1	1.1	1.98
	TOM_3	1	Enameloid	1	1	1.07	1.24
			Enameloid + dentin	1	1	1.09	1.8
	TOM_4	1	Enameloid	1	1	1.03	1.3
			Enameloid + dentin	1	1	1.01	1.84
	TOM_5	1	Enameloid	1	1	1.03	1.24
			Enameloid + dentin	1	1	1.02	1.89
	TOM_6	15	Enameloid + dentin	1	1	1.08	2.02
NIST SRM 120c	NIST120c	1	Phosphate rock	10	11	1.04 ± 0.06	1.16 ± 0.10

9007-34-5) or silver oxide (Ag_2O) crystals to observe FTIR spectra features of pristine and contaminated silver phosphate crystals (**SM5**). Silver oxide crystals were prepared in-house by mixing 300 μL 3 M $AgNO_3$ and 700 μL 2 M NaOH. Crystals were rinsed three times with deionized water and dried overnight. The same crystals were also used for $\delta^{18}O$ analysis to monitor significant isotopic shifts in Ag_3PO_4 crystals due to inclusion of this oxygen-bearing mineral. Finally, we prepared five in-house silver carbonate (Ag_2CO_3) samples to test the degree of isotopic shift due to the incorporation of inorganic contaminants in different amounts, like the apatite structural carbonate. Crystals were precipitated by mixing 0.75 mL 1 M $AgNO_3$ and 0.75 mL 0.5 M $NaHCO_3$. Crystals were rinsed three times with deionized water and dried overnight. All samples were homogenized into a single powder batch.

2.2. Rapid UC precipitation

Phosphate standard materials and biogenic apatite samples were chemically processed with the Rapid UC method after Mine et al. (2017). We weighed ~1.5 mg of each apatite replicates to the nearest 10^{-3} mg (Table 1). Specimens with high organic content (i.e., tooth crown surface/dentin mixture and bone specimens; Table 1) were treated in 300 μL 2.5% NaClO for ~17 h to oxidize organics (Tube A; Fig. 1). Samples were rinsed five times with deionized water (DIW) and dried overnight. All samples were pre-dissolved in 50 μL 2 M nitric acid (HNO_3) overnight (Tube A). To precipitate calcium fluoride (CaF_2), 30 μL 2.9 M hydrofluoric acid (HF) was added, then the solution was buffered with 50 μL 2 M sodium hydroxide (NaOH) (Tube A; Fig. 1). Samples were gently shaken for 120 min and then centrifuged to pellet CaF_2. The supernatant with dissolved phosphate ions was transferred into a clean microcentrifuge tube (Tube B; Fig. 1). The CaF_2 was rinsed with 100 μL 0.1 M sodium fluoride (NaF) to recover phosphate adsorbed on the pellet surface. The CaF_2 crystals were re-centrifuged and the supernatant was transferred into Tube B with the first aliquot of supernatant. Dissolved phosphate was precipitated as Ag_3PO_4 with 180 μL of silver ammine solution, a mixture of 0.37 M silver nitrate ($AgNO_3$) and 1.09 M ammonium hydroxide (NH_4OH) (Fig. 1). We adjusted the pH close to neutrality (pH range between 5.5 and 7.5) by adding small aliquots (~10 μL) of 2 M HNO_3 or 2 M NaOH solution to optimize Ag_3PO_4 precipitation, which lasted ~15 min. The precipitated Ag_3PO_4 crystals were rinsed five times with DIW and dried overnight. All steps were run in 1.75 mL microcentrifuge vials.

2.3. SPORA protocol: decision-making process in establishing the new technique

The new protocol has three components: (i) CaF_2 precipitation, (ii) anion exchange purification, and (iii) Ag_3PO_4 precipitation (Fig. 1). These chemical steps were designed and tested in several preliminary experiments exploring efficiency of phosphate isolation, elution from the resin, and precipitation as silver phosphate. These steps were designed to (i) dissolve bioapatite without using reagent(s) that may interfere during the phosphate adsorption (i.e., nitrate), (ii) purify phosphate from organic and carbonate contamination, and (iii) precipitate phosphate rapidly to minimize coprecipitation of oxygen-bearing minerals (e.g., Ag_2O). Dissolved phosphate concentrations were measured via UV–Vis spectrophotometry in each step, respectively (Mine et al., 2017; Murphy and Riley, 1962) (see Section 2.5 for a detailed description of the application).

2.3.1. Apatite dissolution and CaF_2 precipitation

Many protocols require soaking the apatite powder in a 2 M HF solution for 24 h (Crowson et al., 1991; Lécuyer et al., 1998; Lécuyer et al., 1993; Pederzani et al., 2020; Shabaga et al., 2018; Stephan, 2000; Tütken et al., 2006; Vennemann et al., 2002), whereas others predissolve samples in a 2 M HNO_3 before adding the HF reagent (Dettman et al., 2001; Mine et al., 2017; O'Neil et al., 1994; Wiedemann-Bidlack et al., 2008). We avoided the latter step as NO_3^- ions can interfere with resin affinity for phosphate during the purification step (Bio-Rad Laboratories, 2000; Crowson et al., 1991; Pederzani et al., 2020). A preliminary test on synthetic hydroxyapatite and NIST SRM 120c standards shows that a 300 μL aliquot of 2 M HF solution yields similar amounts of phosphate as the Rapid UC protocol (see **SM2** for a detailed description). Therefore, the SPORA protocol starts with ~1.5 mg apatite powder in a 1.75 mL microcentrifuge tube (Tube A; Fig. 1) with the addition of 300 μL 2 M HF. Samples are soaked for 24 h on a shaker table to complete the dissolution reaction. Once CaF_2 pellets form (Fig. 1), the

phosphate-rich supernatant is pipetted into a clean tube (Tube B; Fig. 1). CaF_2 pellets in Tube A are further rinsed one time with 100 μL with DIW, and the solution is transferred into Tube B.

2.3.2. Anion exchange purification

An anion exchange purification step was included before the Ag_3PO_4 precipitation in order to isolate phosphate from other compounds (e.g., organics or carbonate) that could contaminate silver phosphate crystals. Several protocols used the AMBERLITE™ IRN78 resin in hydroxide form to purify phosphate from organics in slow silver phosphate precipitation protocols (Crowson et al., 1991; Lécuyer et al., 1993; Pederzani et al., 2020; Royer et al., 2013). However, this product does not fit our goals because the resin beads (i) are large (630 ± 50 μm), (ii) contain chlorine ions in their structure (Dupont, 2019a, 2019b), which may be released during the desorption step and precipitate as silver chloride (AgCl) alongside Ag_3PO_4 (Grimes and Pellegrini, 2013; Lécuyer, 2004), and (iii) require circumneutral working solutions to adsorb phosphate, necessitating time-consuming pH adjustments following apatite dissolution. Other protocols for phosphate extraction from soil and water samples use the Dowex (AmberChrom™) 1-X8 anion exchange resin (Andersohn, 1996; Dupont, 2019b; Lapworth et al., 2014; Sibbesen, 1978). However, phosphate adsorption is optimal when the resin is converted into a ~ 75% bicarbonate/~25% chloride form (Sibbesen, 1978) and chlorine/based solutions (either hydrochloric acid or potassium chloride) are often required to elute phosphate (e.g., Sibbesen, 1978; Lapworth et al., 2014). Again, this resin does not fit our requirements due to potential downstream AgCl contamination during later Ag_3PO_4 precipitation.

We scaled the purification step to a 400 μL working volume (see the combined HF solution and deionized water volumes in Section 2.3.1) by using the chloride-free Bio-Rad AG™ 1-X8 anion exchange resin in hydroxide form (Fig. 1). These resin beads prefer small, inorganic, monovalent ions (e.g., phosphate as $H_2PO_4^-$) and are successfully employed in phosphate extraction and elution protocols for water samples (Colman, 2002; Colman et al., 2005; Goldhammer et al., 2011; Goldhammer et al., 2010). Because the resin beads are small (106–180 μm) and sticky, we used Millipore Sigma Ultrafree™ – CL centrifugal tubes with a polytetrafluoroethylene (PTFE) microporous membrane (pore size of 0.2 μm) (Merck KGaA, 2018) to facilitate adsorption and desorption steps. These vials have a 2 mL filter unit that can be removed from the 5 mL collector tube (Tubes B and C, Fig. 1).

We conducted several preliminary experiments to assess the proper working pH, type, and concentration of counter ions to efficiently isolate phosphate from impurities. These results demonstrated that phosphate adsorption to resin is independent of pH and 0.44 M sodium nitrate ($NaNO_3$) is the optimal solution for eluting phosphate (Fig. 1; see **SM3** for a detailed description). The anion exchange purification process in SPORA reflects these optimized conditions. The phosphate-rich supernatant is pipetted into the filter unit pre-loaded with resin (Tube B, Fig. 1). The resin uptakes phosphate in exchange for hydroxide ions (Bio-Rad Laboratories, 2000). Then, the solution is centrifuged down at 4500 RPM for 30 min to the collector tube to isolate dissolved impurities. At this stage, the filter unit is plugged into a clean collector tube (Tube C) to elute phosphate with seven rinses of 200 μL 0.44 M $NaNO_3$ (Fig. 1).

2.3.3. Ag_3PO_4 precipitation

Silver phosphate crystals precipitate when the phosphate-rich solution is combined with a silver ammine solution (Fig. 1) that has high concentration of Ag^+ compared to phosphate (0.37 M $AgNO_3$, Ag^+,PO_4^{3-} ratio ≥10:1) (Mine et al., 2017; O'Neil et al., 1994). The elution of phosphate is achieved using a $NaNO_3$ eluent. The elution process involves transferring the phosphate from the resin into a large working volume of the eluent (1400 μL, **SM3**). It is important to note that this solution also contains water, which may lead to coprecipitation of oxygen-bearing compounds like silver oxide (Ag_2O) given a large amount of hydroxide ions in solution. To avoid Ag_2O contamination while precipitating Ag_3PO_4, the silver ammine solution for SPORA uses 180 μL of a solution containing 0.22 M $AgNO_3$ and 1.09 M NH_4OH (Tube D, Fig. 1). This solution has a lowered $AgNO_3$ concentration compared to that used in the Rapid UC protocol (Mine et al., 2017) (**SM4**).

2.4. Stable oxygen isotope analysis

The $\delta^{18}O_p$ values of silver phosphate crystals were measured with a Thermal Conversion Elemental Analyzer (TC/EA)-ConFlo IV-Delta V Plus continuous flow isotope ratio mass spectrometer system (Thermo Scientific, Bremen, Germany) at the Stable Isotope Ecosystem Laboratory of (SIELO) University of California, Merced (California, USA). Samples were run in triplicates of ~0.2 mg each and were packed into silver capsules. Silver phosphate is reduced to CO gas by heating the TC/EA graphite column at 1450 °C. Drift and linearity correction were applied. Then, samples were calibrated to the Vienna Standard Mean Ocean Water scale (V-SMOW) with a 2-point calibration using Ag_3PO_4 reference materials. The USGS 80 ($\delta^{18}O_p$ = 13.1 ± 0.2‰ (n = 234), United States Geological Survey [USGS]; >99% purity) and USGS 81 ($\delta^{18}O_p$ = 35.4 ± 0.3‰ (n = 231), USGS; >99% purity) are the certified silver phosphate reference materials used to calibrate samples and to assess analytical accuracy and precision. Analytical precision of biogenic and working reference apatite materials are reported as mean ± 1σ.

2.5. UV–Vis spectrophotometry – soluble reactive phosphate measurements

To determine phosphate recovery performance and compare it to isotopic composition, we measured dissolved phosphate concentrations with a molybdate blue spectrophotometric technique. The approach determines the amount of dissolved, inorganic soluble reactive phosphate (SRP) irrespective of phosphate species (i.e., ΣPO_4^{3-}) via formation of a molybdate blue complex (Murphy and Riley, 1962). Phosphate concentrations were determined following acid dissolution (i.e., "starting concentration", *SC*), phosphate adsorption to resin (i.e., "resin step 1", *RS1*), phosphate elution (i.e., "resin step 2", *RS2*), and after Ag_3PO_4 crystal precipitation (i.e., "precipitation", *P*) for the SPORA protocol (Fig. 1). Similarly, samples processed with the Rapid UC method were measured for phosphate concentration following apatite dissolution and crystal precipitation (i.e., aliquots *SC* and *P*, Fig. 1).

Aliquots were diluted up to a 5000-fold factor to constrain the phosphate concentration of samples within the absorbance-concentration linear response range given by the potassium dihydrogen phosphate (KH_2PO_4)-based standard curve (0 to 20 μM phosphate). Diluted samples were mixed with the colorimetric reagent made of a mixture of 2.5 M sulfuric acid (CAS: 7664-93-9), 24 mM ammonium molybdate tetrahydrate (CAS: 12054–85-2), 0.31 M ascorbic acid (CAS: 50–81-7), and 2 mM antimony potassium tartrate (CAS: 331753–56-1) in a 5:2:2:1 volume ratio, respectively (Mine et al., 2017). Because residual silver may interfere with the colorimetric reagents, aliquots collected after the precipitation (i.e., aliquots *P* in Fig. 1) were treated with a 1 M sodium chloride (NaCl) solution to remove Ag^+ as AgCl (Mine et al., 2017). Additionally, we matched standard curve matrices to samples, ensuring solution compositions were the same.

Absorbance values were measured with a Thermo Scientific Evolution 300 (Thermo Fisher Scientific) spectrophotometer equipped with a xenon lamp set at 883 nm housed in the Ghezzhei Lab of Soil Physics at the University of California, Merced (California, USA). We checked potential departures of absorbance accuracy by comparing KH_2PO_4-based standard curves generated at each run. Finally, we monitored the fraction of phosphate moles at each chemical step and calculated the phosphate recovery (ΣPO_4^{3-} (%)) relative to the initial amount of dissolved phosphate. The total phosphate recovery for the SPORA protocol was calculated as follows:

$$\sum PO_{4\ SPORA}^{3-}\ (\%) = \left(\left(\sum PO_{4\ RS2}^{3-} - \sum PO_{4\ P}^{3-}\right) \Big/ \sum PO_{4\ SC}^{3-}\right) * 100$$

where $\Sigma PO_{4\ RS2}^{3-}$ is the phosphate amount following phosphate elution (Tube C), $\Sigma PO_{4\ P}^{3-}$ is the residual amount after the precipitation, and $\Sigma PO_{4\ SC}^{3-}$ is the starting amount of dissolved phosphate. Because the Rapid UC has two major steps (Fig. 1), phosphate recovery was calculated as follows:

$$\sum PO_{4\ Rapid\ UC}^{3-}\ (\%) = \left(\left(\sum PO_{4\ SC}^{3-} - \sum PO_{4\ P}^{3-}\right) \Big/ \sum PO_{4\ SC}^{3-}\right) * 100$$

2.6. FTIR analysis

We used Fourier-Transform Infrared Spectroscopy (FTIR) to evaluate the material composition of crystals precipitated with both protocols and their corresponding apatite materials. If contaminated, FTIR spectra of Ag_3PO_4 crystals would show infrared-active vibrational bands of nitrogen-based compounds, silver-oxygen, silver-carbonate, or a mixture of both along with absorption bands of phosphate groups. Such bands are produced via the inclusion of amide groups from collagen, silver oxide, and silver carbonate particles in silver phosphate crystals (Al Sekhaneh et al., 2021; Grunenwald et al., 2014; Haq et al., 2018; Köck et al., 2013; Kumar and Rani, 2013; Lebon et al., 2016; Oje et al., 2019; Rahman et al., 2018; Rashmi et al., 2020; Shimabukuro et al., 2022; Siddiqui et al., 2013; Slager et al., 1972; Suthanthiraraj and Sarumathi, 2012; Suwanprateeb et al., 2012; Trayler et al., 2023; Trivedi et al., 2015). For reference spectra, we analyzed the material composition of silver phosphate (>99% purity, Alfa Aesar) mixed with ~20%wt of collagen standard or Ag_2O to verify vibrational modes of these functional groups (**SM5**).

Before FTIR analysis, replicates of silver phosphate crystals precipitated from a specific apatite material and protocol were combined to improve sample size. Thus, all silver phosphate spectra show the average molecular composition when precipitated with a specific protocol. Spectra were collected with a Bruker Vertex 70 Far-Infrared in ATR mode held by the Nuclear Magnetic Resonance Facility at the University of California, Merced (California, USA). Spectra were collected within 400–4000 cm^{-1} and were smoothed by overlapping 32 scans of the same sample at a resolution of 4 cm^{-1}. We corrected spectra to level down the baseline of absorbance bands. The correction fits several spline curves to subtract the background at points with expected absorbance intensity equal to 0 following R code scripts published elsewhere (RStudio Team, 2021; Trayler et al., 2023).

2.7. Exploration of silver oxide and carbonate

We measured $\delta^{18}O$ values of in-house precipitated silver oxide (Ag_2O) and carbonate (Ag_2CO_3) to monitor the deviation of Ag_3PO_4 oxygen isotope composition due to coprecipitation of these two oxygen-bearing compounds. Replicates of Ag_2O ($n = 8$) and Ag_2CO_3 ($n = 22$) were packed into silver capsules and $\delta^{18}O$ values were measured as described in Section 2.4.

We tested the isotopic effect of inorganic carbonate contamination (e.g., structural carbonate) as silver carbonate inclusion by simulating Ag_2CO_3 – Ag_3PO_4 mixtures in varying silver carbonate quantities (i.e., ~1 to ~10%wt Ag_2CO_3). The Ag_3PO_4 substrate of the simulated mixtures derives from the working fluorapatite reference that was treated with both protocols (n = 22; Tables 1 and 2). We ran 10,000 simulations to estimate the degree of isotopic shift in contaminated Ag_3PO_4 crystals using the following equation:

$$\delta^{18}O_{mix} = \left(\delta^{18}O_p * Ag_3PO_{4\ wt\%}\right) + \left(\delta^{18}O_{Ag_2CO_3} * Ag_2CO_{3\ wt\%}\right)$$

where $\delta^{18}O_p$ and $Ag_3PO_{4\ wt\%}$ are the isotopic composition and fraction of Ag_3PO_4 in the mixture, $\delta^{18}O_{Ag2CO3}$ and $Ag_2CO_{3\ wt\%}$ are the isotopic composition and fraction of Ag_2CO_3 in the mixture, and $\delta^{18}O_{mix}$ is the isotopic composition of the Ag_2CO_3 – Ag_3PO_4 mixture.

Finally, we compared contaminated $\delta^{18}O$ values from the simulations to measurements of manually contaminated silver phosphate. The $\delta^{18}O_{mix}$ values are from Ag_3PO_4 crystals ($n = 13$) that were manually contaminated with Ag_2CO_3 aliquots to ensure agreement between simulations and empirical values. We used Ag_3PO_4 crystals precipitated from the working fluorapatite reference material via Rapid UC protocol as substrate for the mixture. Each sample was homogenized with varying Ag_2CO_3 fractions between ~1 and ~10%wt. All samples were run in triplicates of ~0.2 mg and packed into silver capsules for oxygen isotope analysis in the TCEA as described above.

3. Results and discussion

3.1. SPORA and Rapid UC protocols yield similar $\delta^{18}O_p$ values

We developed a new silver phosphate precipitation procedure, the SPORA protocol, that closely preserves the phosphate oxygen isotope composition of biogenic and reference apatite materials. The $\delta^{18}O_p$ measurements of apatite materials treated with SPORA and the Rapid UC protocols have high, linear correlation with a 1:1 linear regression ($R^2 = 0.99$; $p << 0.05$; Fig. 2). Notably, reference materials and low-organic content specimens such as tooth enameloid and enamel from modern samples exhibit the highest agreement between protocols. These

Table 2
The $\delta^{18}O_p$ values for the Rapid UC and SPORA protocols are compared across a range of biogenic apatites, reference materials, and phosphatic standards. Several specimens were sampled multiple times for different material types (i.e., enamel(oid) vs. dentin). The variation between protocols ($\Delta^{18}O$) is represented as the difference between mean values ($\delta^{18}O_{p\ SPORA}$ - $\delta^{18}O_{p\ Rapid\ UC}$). The uncertainty around the mean difference between protocols is represented by the standard error. The column "Type" reports whether samples are working standard materials (S) or biogenic apatite materials with expected low- (LOC) or high-organic content (HOC).

Sample	Material	ID	Type	$\delta^{18}O_{p\ Rapid\ UC}$ (‰)	$\delta^{18}O_{p\ SPORA}$ (‰)	$\Delta^{18}O$ (‰)
Fossil mammal indet.2	Bone	MM2	HOC	14.5 ± 0.1	13.7 ± 0.1	−0.7 ± 0.1
Modern deer	Bone	OV	HOC	16.2 ± 0.3	15.6 ± 0.2	−0.5 ± 0.2
Fossil mammal indet.1	Bone (tar not removed)	MM1	HOC	NA	17.3 ± 0.2	NA
	Bone (tar removed)	MM1		17.7 ± 0.3	17.8 ± 0.1	0.0 ± 0.1
Fluorapatite	Naturally occurring crystal	FA	R	9.0 ± 0.4	8.8 ± 0.3	−0.2 ± 0.2
Modern goat	Enamel	CH	LOC	14.1 ± 0.2	14.2 ± 0.2	0.1 ± 0.1
	Enamel + dentin	CH	HOC	12.8 ± 0.1	12.4 ± 0.2	−0.4 ± 0.1
Fossil shark	Enameloid	SM1	LOC	17.4 ± 0.2	16.9 ± 0.4	−0.5 ± 0.2
	Enameloid + dentin	SM1	HOC	13.8 ± 0.3	13.6 ± 0.4	−0.2 ± 0.2
Fossil shark	Enameloid	SM2	LOC	8.0 ± 0.3	7.8 ± 0.5	−0.2 ± 0.3
	Enameloid + dentin	SM2	HOC	9.7 ± 0.1	9.4 ± 0.2	−0.2 ± 0.1
Modern shark	Enameloid	TOM	LOC	22.7 ± 0.2	22.4 ± 0.3	−0.3 ± 0.2
	Enameloid + dentin	TOM	HOC	23.3 ± 0.3	22.4 ± 0.3	−0.9 ± 0.2
NIST SRM 120c	Phosphate rock	NIST120c	R	21.9 ± 0.1	21.7 ± 0.3	−0.2 ± 0.1
Hydroxyapatite	Synthetic crystal	HAP	R	22.2 ± 0.2	21.8 ± 0.3	−0.4 ± 0.1

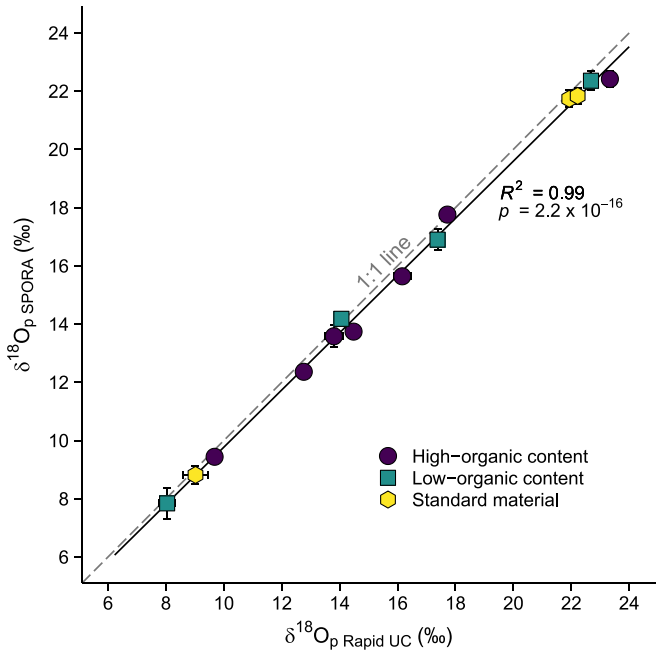

Fig. 2. The mean $\delta^{18}O_p$ values of standard and biogenic apatite materials converted into Ag_3PO_4 crystals with SPORA and Rapid UC methods are equivocal. Both protocols yield similar oxygen isotope compositions and plot along a 1:1 line (shown in gray; ($R^2 = 0.99$; $p = 2.2 \times 10^{-16}$). Error bars represent the uncertainty of measurements as 1σ. Point shapes and color show whether crystals are precipitated from working standard materials or from biogenic apatite materials with expected low- or high-organic content. See Results and Discussion section for samples that vary.

specimens show $\delta^{18}O_p$ values within the accepted analytical error (~0.3‰) when comparing protocol performances (Fig. 2; Table 2), indicating similarity between treatment outcomes.

Divergences between treatments arise in samples with higher organic content or diagenetic alteration. Fossil specimens, the modern deer bone, and tooth mixtures are indeed those that behave differently. Apatite materials of modern specimens with expected high organic contents, such as tooth crown surface and dentin mixtures or bone specimens (OV and MM2) show a larger isotopic offset between protocols ($\Delta^{18}O$, $\delta^{18}O_{p\ SPORA}$ - $\delta^{18}O_{p\ Rapid\ UC}$) ranging from -0.4 ± 0.1‰ to -0.9 ± 0.2‰ (Fig. 2; Table 2). The fossil bone MM1 has similar $\delta^{18}O_p$ values between protocols if tar is removed, but an isotopic shift of ~ −0.5‰ is observed when comparing the untreated and the tar-removed powder precipitated with SPORA protocol. Finally, the enemaloid of the shark specimen SM1 has a $\Delta^{18}O$ offset of ~ − 0.5‰ (Table 2). The isotopic composition of fossil shark tooth mixtures is quite different from that of pure enameloid within the same tooth specimen regardless of the protocol used. This difference ranges from ~1.6‰ in SM2 to ~3‰ in SM1 specimen (Table 2) and is likely due to diagenetic alteration or variably isotopic composition between tissues.

Overall, both protocols yield similar isotopic values when using apatite materials with expected low or no organic content, while protocols perform differently on samples with expected high amounts of collagen or fossil materials with diagenesis. Five possible explanations for protocol differences are: (i) SPORA contains contamination derived from the used reagents; (ii) SPORA successfully isolates phosphate from organics; (iii) incomplete Ag_3PO_4 precipitation affects isotopic fractionation; (iv) isotopic heterogeneity in samples generates apparent isotopic effects; (v) protocols behave differently if samples are diagenetically altered.

3.2. SPORA mitigates Ag_2O contamination in Ag_3PO_4 crystals

Infrared spectra detected the nature of contamination in precipitated Ag_3PO_4 crystals (Fig. 3) that caused the observed isotopic variation between protocols (Table 3 and **SM5**). All crystals show sharp ν_4PO_4 and ν_3PO_4 absorption bands at 542 and 930 cm^{-1}, and small peaks also occur at 603 and 1095 cm^{-1}, respectively. A small oxygen-silver-oxygen band occurs in crystals precipitated with the Rapid UC method at ~1072 cm^{-1} (Fig. 3), which we interpreted as Ag_2O inclusion (Fig. 3). No silver oxide infrared band is shown in crystals precipitated with SPORA protocol (Fig. 3).

These observations suggest that the Rapid UC protocol incorporates Ag_2O during precipitation of Ag_3PO_4 crystals. This is likely due to the higher concentration of silver used to promote Ag_3PO_4 precipitation (see **SM4**) (Mine et al., 2017). Water and/or air are the likely oxygen sources in Ag_2O (Biedermann et al., 1960; Charlot, 1969):

$$Ag^{+}_{(aq)} + OH^{-}_{(aq)} \rightarrow AgOH_{(s)} \rightarrow {}^{1}/_{2}\ Ag_2O_{(s)} + {}^{1}/_{2}\ H_2O_{(aq)}$$

The mean oxygen isotope value from our in-house precipitated Ag_2O (0.4 ± 1.7‰; **SM9**) likely reflects the isotopic composition of the silver oxide contamination in Ag_3PO_4 crystals precipitated via Rapid UC procedure. These values suggest that incorporation of Ag_2O introduces ^{16}O-enrichments that may cause a shift toward low $\delta^{18}O_p$ values. However, Ag_2O contamination alone cannot explain variability in $\delta^{18}O_p$ values between protocols. Such shift should be systematic in all crystals precipitated via Rapid UC method regardless of the nature of the starting material, which is not the case (Fig. 2 and Table 2). Again, the greatest variability occurs with apatite materials high in organic content and in fossil specimens.

3.3. SPORA contains the inclusion of organic-altered carbonate as silver carbonate (Ag_2CO_3)

No crystals show amide vibration bands (Fig. 3), indicating that anion exchange resin and bleach removed nitrogen-rich organic fraction or they are below detection limits in agreement with other studies (Grimes and Pellegrini, 2013; Pederzani et al., 2020; Wiedemann-Bidlack et al., 2008). Instead, silver carbonate is likely a contaminant phase for most silver phosphate methods. Infrared absorption occurs at ~1405 and 1545 cm^{-1}, which are modes of carbonate functional groups (Fig. 3; see also **SM5**). Carbonate peaks are small for both protocols, but the SPORA method produces crystals with a slightly larger ν_3CO_3 band at 1545 cm^{-1} (**SM8**), which is likely due to structural carbonate, an inevitable confounding factor in Ag_3PO_4 precipitation methods.

The inclusion of carbonate may be strictly related to its source types and conversion into different species (i.e., CO_2, HCO_3^-, CO_3^{2-}) as pH varies (Abderrahim et al., 2016). There are a variety of sources for carbonate that could potentially contaminate Ag_3PO_4 crystals. First, oxidized metals such as Ag_2O or reagents like the silver ammine solution may absorb atmospheric or dissolved CO_2 from the headspace of vials (L'vov, 1999; Mine et al., 2017; Slager et al., 1972; Trivedi et al., 2015) (see also **SM5**). Second, structural carbonate precipitates as a substitute for phosphate and hydroxide (or fluorine in shark enameloid) crystallographic sites during apatite mineralization (Enax et al., 2014; Enax et al., 2012; LeGeros, 1981; Leventouri, 2006) (see also **SM6**). Lastly, carbonate could be an unwanted effect as a result of organic degradation (Crowley and Wheatley, 2014; Grimes and Pellegrini, 2013).

If samples contain low or no organic content, structural carbonate and/or atmospheric CO_2 are likely the main source of contamination for both protocols. When apatite materials are dissolved in weak acid solutions like the HF reagent (pH ~ 1; Fig. 1), structural carbonate is released as free gas (Abderrahim et al., 2016) that could equilibrate with the solvent forming dissolved carbon dioxide (CO_2) at standard temperature and pressure conditions (Cox and Head, 1962). For example, assuming that 1 mg of bioapatite yields 6%wt carbonate (Crowley and

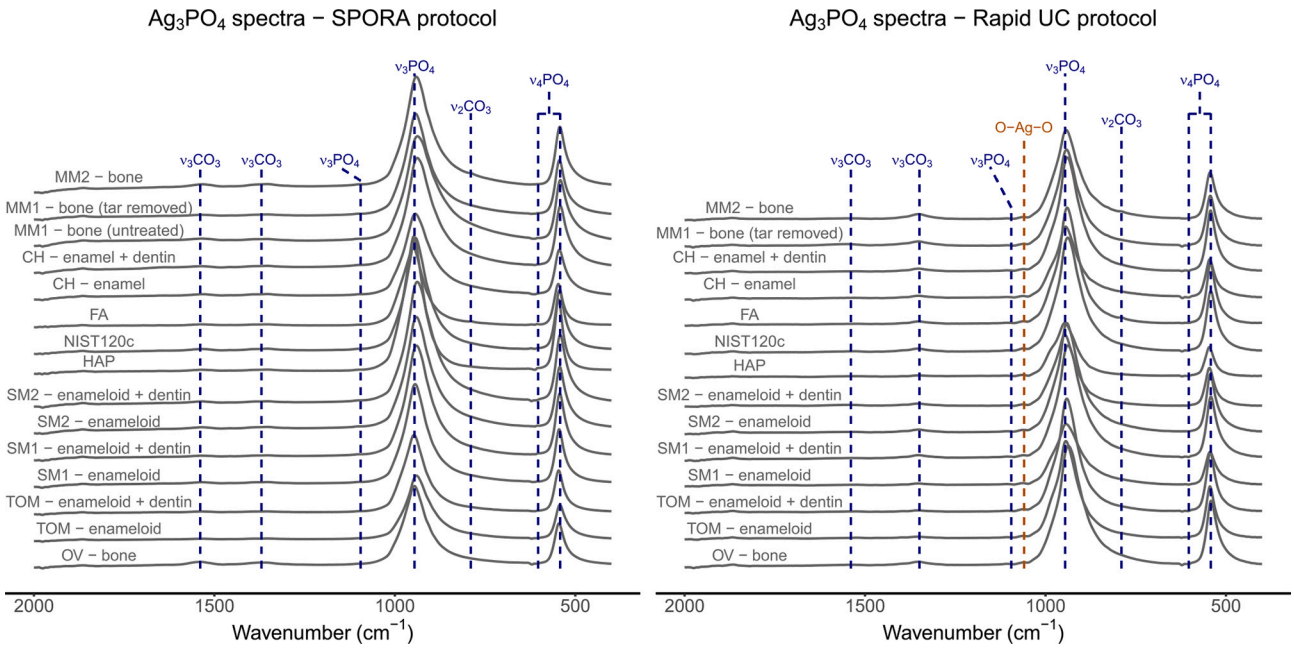

Fig. 3. The SPORA protocol prevents the inclusion of Ag_2O and mitigates carbonate contaminants as demonstrated by FTIR spectra. The left panel shows infrared spectra of Ag_3PO_4 crystals produced with the SPORA protocol, whereas the right panel displays spectra of the same apatite specimens treated with the Rapid UC method. Crystals precipitated with both protocols show similar phosphate and carbonate infrared features. Silver phosphate crystals precipitated via Rapid UC method show silver oxide bands.

Table 3
Soluble reactive phosphate was measured for SPORA and compared to UC Rapid to determine phosphate recovery (ΣPO_4^{3-} (%)) at key points of possible loss in the protocol. The summary statistics include median, interquartile range (IQR), mean, and standard deviation values are reported.

Protocol	ΣPO_4^{3-} (%)			
	# Replicates	median	IQR	mean ± sd
Rapid UC	91	97.8	3.9	96.3 ± 5.4
SPORA	95	91.2	12.8	89.2 ± 9.6

Wheatley, 2014), a Henry's law constant for CO_2 (K_{CO2}) of 0.0357 mol * L^{-1} atm^{-1} for a 2.5 M HF solution (Cox and Head, 1962), and 300 μL of solvent in a 1.5 mL capped vial (i.e., close system), about 21% of the carbon dioxide gas yielded from the structural carbonate dissociation could stay dissolved in the reagent (full calculation is found in **SM10**). In strong acid media like the HNO_3 initially used in the Rapid UC protocol, the structural carbonate pool should evolve as CO_2 gas and have no interaction with the solution. Bicarbonate (HCO_3^-) would also form because silver ammine solutions are always prepared to change the pH close to neutrality (Abderrahim et al., 2016; Mine et al., 2017; O'Neil et al., 1994) (see also **SM4**). As a result, the remaining silver ions coprecipitate silver carbonate (Ag_2CO_3) given the following chemical equilibria (Abderrahim et al., 2016; Atwater, 2002; Barnes et al., 1971):

$$CO_{2(aq)} + H_2O_{(aq)} \rightleftharpoons H_2CO_{3(aq)} \rightleftharpoons HCO^-_{3(aq)} + H^+_{(aq)}$$
$$HCO^-_{3(aq)} + H^+_{(aq)} \rightleftharpoons CO^-_{3(aq)} + 2H^+_{(aq)}$$

$$Ag_2O_{(s)} + CO_{2\ (aq\ or\ g)} \rightarrow Ag_2CO_{3\ (s)}$$

$$2AgNO_3{}^+{}_{(s)} + H_2CO_{3\ (aq)} \rightarrow 2AgNO_3{}^+{}_{(s)} + HCO_3{}^-{}_{(aq)} + H^+{}_{(aq)} \rightarrow Ag_2CO_{3\ (s)} + 2HNO_{3\ (aq)}$$

Inclusions of mainly structural carbonate and/or atmospheric CO_2 into Ag_3PO_4 crystals could explain why protocols show low $\Delta^{18}O$ offset for these types of materials. However, there is added complexity when using bones or teeth with high collagen content. When exposing bone and tooth mixtures to NaOCl solution (pH = 9.5; Fig. 1, Rapid UC protocol), amide groups undergo decomposition but bleach does not remove completely the organic fabric (Grimes and Pellegrini, 2013; Gu et al., 2017; Marending et al., 2007; Snoeck and Pellegrini, 2015). Amino acids that survive to bleach, such as glycine and alanine, adsorb CO_2 under circumneutral pH conditions (Guo et al., 2013). If this occurs during Ag_3PO_4 precipitation, ^{18}O-depleted CO_2 molecules could be adsorbed from the vial headspace, leaving the heavier isotopologues behind. The ^{18}O-enriched CO_2 in the headspace will be adsorbed by the silver ammine solution (Mine et al., 2017) and promote ^{18}O-enriched Ag_2CO_3 coprecipitation. This mechanism could offer insights into the consistent presence of Ag_2CO_3 contamination across samples (Fig. 3, **SM8**), where the crucial factor is how organics influence modifications to atmospheric CO_2 in the vial headspace. Indeed, samples showing high organic content subjected to bleach pretreatment exhibit isotopic shifts higher than 0.3‰ compared to samples treated via SPORA or their corresponding enameloid materials processed with Rapid UC (Fig. 2, Table 2, **SM6**).

In contrast, the SPORA protocol does not use a NaOCl pretreatment and isolates phosphate from collagen with an anion exchange resin, preventing undesired isotopic shifts during the Ag_3PO_4 precipitation. SPORA dissolves samples in HF, a weak acid where collagen proteins break down into simple amino acids polarized with positively charged organic compounds ($R\text{-}NH_3^+$) (Bowes et al., 1955; Liu and Huang, 2016; Nishiyama et al., 2003). These organic compounds should have no interactions with an anion exchange resin. As a result, we speculated that the SPORA protocol produces Ag_3PO_4 with more accurate measurements by preventing the inclusion of organic-altered carbonate. The exclusion of this proposed carbonate contaminant is key to precipitating Ag_3PO_4 crystals with $\delta^{18}O_p$ values closer to the actual phosphate isotopic composition of biogenic apatite materials. This hypothesis is also supported by $\delta^{18}O_p$ values of enameloid and tooth mixtures in modern shark teeth, where the SPORA protocol yields very similar values between mixed substrate material types (i.e., enameloid and dentin) compared to the Rapid UC method (Fig. 2 and Table 2). Therefore, inorganic structural carbonate and/or unaltered atmospheric CO_2

should be the main contaminant in Ag_3PO_4 crystals precipitated with the SPORA protocol.

Although the SPORA protocol produces Ag_3PO_4 crystals with slightly more carbonate contamination than the Rapid UC method (Fig. 3 and **SM8**), such contamination does not cause a significant shift in $\delta^{18}O_p$ values. Our experimental test on simulated and manually created Ag_2CO_3-Ag_3PO_4 mixtures (Fig. 4) demonstrates the potential ~13‰ offset ($\delta^{18}O_{p\ Fluorapatite} = 8.9 \pm 0.4$‰; $\delta^{18}O_{Ag2CO3} = 21.6 \pm 0.7$‰) observed in some taxa (e.g., sharks, small rodents, and lagomorphs) (Karnes et al., 2024; Tütken et al., 2006; Vennemann et al., 2001a, b). The choice of the fluorapatite working reference material used in this experiment is justified by the fact that *i*) it is the material with the least amount of carbonate in its structure (**SM6**) and *ii*) $\delta^{18}O_p$ values and FTIR carbonate peaks are equivocal between protocols (Fig. 2, Fig. 3, Table 2, **SM8**). Both simulated and empirical values largely agree that inclusions of 1.5%wt Ag_2CO_3 or higher cause a shift toward higher $\delta^{18}O$ values, making measurements inaccurate (Fig. 4). Given that protocols yield similar $\delta^{18}O_p$ values (Fig. 2 and Table 2), we speculate that the Ag_2CO_3 fraction in Ag_3PO_4 crystals produced with the SPORA technique is below this threshold.

3.4. SPORA protocol recovers less phosphate than Rapid UC with no isotope effects

Contrary to the Rapid UC method, the SPORA protocol requires more wet chemistry steps to treat phosphate (Fig. 1). Anion exchange purification and precipitation steps to isolate, extract, and precipitate phosphate could increase losses of dissolved phosphate relative to the starting amount. Incomplete resin exchange coupled with incomplete crystal precipitation may lead to isotopic fractionation by altering the original phosphate oxygen isotopologue ratios. Fractionation effects may also occur particularly when the total amount of phosphate recovered is <95% (Mine et al., 2017).

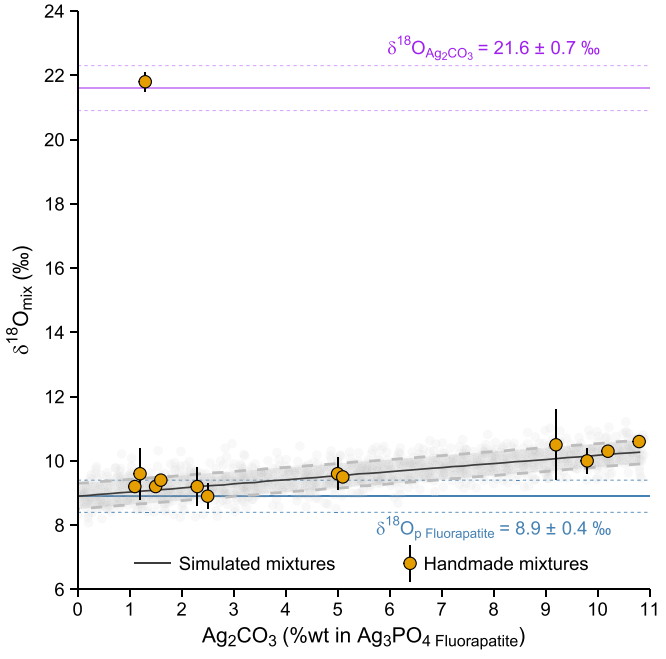

Fig. 4. Inaccurate $\delta^{18}O$ values occur if the inorganic carbonate contaminant fraction as Ag_2CO_3 is ~1.5 wt% or higher. The gray lines show $\delta^{18}O$ values ($\delta^{18}O_{mix}$) by drawing 10,000 simulations of contaminated Ag_3PO_4 crystals considering varying Ag_2CO_3 fractions with an isotopic composition of 21.6 ± 0.7‰ (purple lines). The silver phosphate substrate for the simulated values uses $\delta^{18}O_p$ measurements of working fluorapatite by combining results from both SPORA and Rapid UC protocols (8.9 ± 0.4‰, n = 22, blue lines). Orange dots show $\delta^{18}O_{mix}$ values of Ag_3PO_4 crystals precipitated from the fluorapatite working standard via Rapid UC protocol that were manually contaminated with varying Ag_2CO_3 aliquots. All dashed lines and shaded areas indicate intervals within ±1σ. (For interpretation of the references to color in this figure legend, the reader is referred to the web version of this article.)

UV–Vis spectrophotometry measurements show that increasing the number of wet chemistry steps results in less phosphate recovered. Phosphate recovery distributions of Rapid UC and SPORA protocols are skewed, but the Rapid UC shows a smaller interquartile range (3.9% for Rapid UC and 12.8% for SPORA) compared to the SPORA protocol (Table 3). The latter has a median value of 91.2% against 97.8% of the Rapid UC (Table 3), and this difference is statistically significant (Kruskal-Wallis test, $p = 1.264 \times 10^{-8}$). Overall, these data show that the SPORA protocol recovers on average ~ 90% of dissolved phosphate and recovery is highly variable (Table 3). Among chemical steps, our observations show that resin desorption causes the highest loss and variability in phosphate recovery, where ~10% of phosphate is lost after this chemical step (**SM3** and **SM7**).

Despite the SPORA protocol recovering less phosphate than the Rapid UC protocol, our results suggest that phosphate recovery alone does not explain the variability in $\delta^{18}O_p$ values. If recovery were the cause of isotopic fractionation, a persistent and variable offset in $\delta^{18}O_p$ values between protocols would be evident, but the greatest variability occurs with apatite materials containing high organic content, such as bone samples and tooth crown surface/dentin mixtures of modern specimens (Fig. 2 and Table 2). As such, our results do not support the hypothesis that phosphate recovery with the SPORA protocol has an isotopic effect.

3.5. Specific concerns with shark teeth

We developed SPORA to use on shark teeth given the challenges to analyzing small, fossil specimens. Tooth enameloid and dentin in sharks incorporate oxygen isotopes during the early stages of tooth apatite formation. Sharks do not remodel their teeth once they are fully mineralized, but they continuously replace them in a conveyor belt-like fashion across their life (Dorozhkin, 2009; LeGeros, 1981; Pucéat et al., 2010; Vennemann et al., 2001). Assuming a homogeneous isotopic composition in their apatite structure in both enameloid and dentin within a single tooth and tooth rows, we tested SPORA's performance on shark teeth to address the following hypotheses: *i*) no difference between protocols in $\delta^{18}O_p$ values when using only enameloid; *ii*) tooth enameloid/dentin mixtures yield different $\delta^{18}O_p$ values among protocols; *iii*) no $\delta^{18}O_p$ offset between enameloid and enameloid/dentin mixture when using SPORA.

We initially tested the SPORA protocol on modern shark teeth that indicated offset between protocols due to organic contamination (Table 2). However, this is not the case for fossil shark tooth specimens. The shape of FTIR spectra for tooth enameloid and tooth mixtures of both fossil specimens are indistinguishable (**SM6**), suggesting that organics degraded during the time of fossilization (Ramírez-Bommer et al., 2018). Instead, we ascribed such discrepancies between protocols and between tooth tissues (Table 2) to heterogeneities similar to those observed in mammal teeth. In sharks, apatite mineralization in tooth dentin occurs after the enameloid is fully mature (Enax et al., 2014; LeGeros, 1981; Sasagawa, 1999). Tooth replacement rates are species-specific and can be as slow as 190 days per row tooth series (Botella et al., 2009). In contrast to teeth from the modern blue shark, the fossil sand tiger shark individuals could have slow tooth mineralization rates while experiencing varying environmental conditions, causing isotopic zonation within the enameloid and between enameloid and dentin. Several previous studies have also shown that shark teeth may differ by as much as a few per mille from one area to another and between tooth tissues (Vennemann et al., 2001; Žigaite and Whitehouse, 2014). Therefore, the isotopic differences among the samples from a single fossil specimen could be biologically mediated rather than an artifact of silver phosphate precipitation protocol.

3.6. SPORA protocol's limitations: natural asphalt and diagenetic carbonate removal

The analysis of fossil mammal bones offers a valuable case study to explore limitations of the SPORA protocol with respect to two exogenous contaminants: natural asphalt and diagenetic carbonate (Table 2; **SM6**). Although FTIR analysis on MM1 failed to detect the asphalt component in the untreated specimen (**SM6**), we speculated that the high isotopic offset between tar-removed and untreated sample (Table 2) is due to tar-derived carbonate formed during the HF dissolution step that the anion exchange resin cannot isolate properly and, eventually, interacts with the silver ammine solution during the Ag_3PO_4 precipitation reaction. Natural asphalt is a complex polymer that includes organics with methyl (-CH_3), hydroxyl (-OH), and ether bonds such as aromatic compounds and fulvic acid. These molecules undergo weak oxidation and release CO_2 when exposed to acidic solutions like the HF reagent (Ni et al., 2022; Xue et al., 2019; Yürüm et al., 1985; Zhang et al., 2016, 2020, 2021). The free CO_2 gas could dissolve in the supernatant and interact subsequently with the resin during the phosphate adsorption step. As a result, we recommend using an asphalt removal procedure on tar-contaminated specimens before preparing samples for phosphate oxygen isotope analysis, regardless of whether samples are purified with anion exchange resin or not.

The infrared spectrum of specimen MM2 bone powder displays alteration features due to calcium carbonate inclusion ($CaCO_3$; **SM6**). Inclusions of secondary carbonate sources may shift measurements toward ^{18}O-depleted isotopic values (Garvie-Lok et al., 2004; Koch et al., 1997; Zazzo et al., 2004), a pattern we saw in Ag_3PO_4 crystals precipitated via SPORA procedures when comparing protocols (Table 2). Infrared spectra show more pronounced carbonate peaks for the SPORA protocol (Fig. 3, **SM8**) and an additional carbonate band at 870 cm^{-1} (ν_2CO_3), a feature that is unique to Ag_3PO_4 crystals for this bone specimen in both protocols (Fig. 3). Such carbonate source should not impact the purity and isotopic composition of crystals precipitated via Rapid UC because samples are dissolved in a HNO_3 solution (pH ~ 0) and diagenetic carbonate readily forms free CO_2. Carbon dioxide-trapping bubbles should break apart as the supernatant is agitated and transferred in another vial during the following steps (Fig. 1) but some could also reach stability with the solution in low pH conditions (Tabor et al., 2011). These bubbles could eventually coalesce and dissolve the trapped CO_2 in the supernatant at circumneutral pH (Tabor et al., 2011), a condition achieved when the silver ammine solution is added to precipitate Ag_3PO_4 crystals. This mechanism could explain the occurrence of small ν_2CO_3 bands in Ag_3PO_4 crystals precipitated via Rapid UC method, but, again, diagenetic carbonate has a limited impact on Ag_3PO_4 the isotopic composition given that samples were dissolved in a strongly acidic medium and most of the bubbles formed during the dissolution step should break apart. For diagenetically altered samples like MM2 treated via SPORA method, we recommend removing secondary carbonate minerals like $CaCO_3$ before the procedure given its reaction in HF solution (see also Section 3.4 and **SM10**) or CO_2 bubbles may stabilize in the supernatant (Tabor et al., 2011); in both cases, the CO_2 gas could interact with the resin during the phosphate adsorption step. A possible pretreatment is soaking the stock powder in a 1 M acetic acid buffered with calcium acetate solution. The reagent dissolves secondary carbonates with minor effects on apatite integrity and oxygen isotopes as described elsewhere (Crowley and Wheatley, 2014; Garvie-Lok et al., 2004; Koch et al., 1997).

4. Conclusions

We have designed a new Ag_3PO_4 precipitation protocol (SPORA) for phosphate oxygen isotope analysis that accounts for small sample sizes (i.e., 1.5 mg or less) and collagen contamination. The SPORA protocol performs very closely to current methodologies in terms of oxygen isotope measurements of the Ag_3PO_4 crystals precipitated from different apatite specimens. The use of the anion exchange resin in the SPORA protocol decreases the phosphate recovery to around 90% without causing isotopic shifts in the Ag_3PO_4 crystals. The SPORA protocol minimizes Ag_2CO_3 contamination and prevents the inclusion of Ag_2O and collagen-altered carbonate in Ag_3PO_4 crystals even in organic-rich, crushed, shark tooth samples. While bleach pretreatment to remove collagen is unnecessary when using the SPORA protocol, pretreatments to remove exogenous contaminants like tar or diagenetic carbonate are recommended.

Further, this study is the first to identify secondary oxygen-bearing phases included in Ag_3PO_4 crystals and place them in context to assess the analytical accuracy and precision of $\delta^{18}O_p$ measurements. Deviations from expected $\delta^{18}O_p$ values may occur when contaminants like Ag_2O and Ag_2CO_3 coprecipitate with Ag_3PO_4, the latter being a confounding factor for most silver phosphate protocols to date. Specimens with high collagen content or those being diagenetically altered are the ones that show isotopic shifts higher than ~0.3‰ between different treatments. More experiments on the contribution of each carbonate source to the bulk carbonate contamination as Ag_2CO_3 inclusion are needed in order to test the performance between protocols with respect to isotopic fidelity and Ag_3PO_4 crystal purity.

Current silver phosphate precipitation protocols are faster for samples with low or no expected collagen content or when large samples are available. However, pretreating organic-rich samples with bleach causes undesirable ^{18}O-enrichment as shown in other studies. Samples with a low starting amount of material and high collagen content require an anion exchange purification step to effectively remove organic contaminants (i.e., collagen). The SPORA method isolates phosphate from collagen contamination and enhances the reliability of $\delta^{18}O_p$ measurements, making the application suitable for bioapatite materials of varying organic content, including crushed tooth specimens, for paleoenvironmental, palaeoecological, and archeological applications.

CRediT authorship contribution statement

Gabriele Larocca Conte: Writing – review & editing, Writing – original draft, Visualization, Validation, Supervision, Software, Resources, Project administration, Methodology, Investigation, Formal analysis, Data curation, Conceptualization. **Lauren E. Lopes:** Writing – review & editing, Writing – original draft, Software, Methodology, Investigation, Formal analysis, Data curation, Conceptualization. **Aric H. Mine:** Writing – review & editing, Writing – original draft, Visualization, Validation, Supervision, Resources, Methodology, Investigation, Formal analysis, Conceptualization. **Robin B. Trayler:** Visualization, Validation, Software, Resources, Methodology, Investigation, Formal analysis, Data curation. **Sora L. Kim:** Writing – review & editing, Writing – original draft, Visualization, Validation, Supervision, Software, Resources, Project administration, Methodology, Investigation, Funding acquisition, Formal analysis, Data curation, Conceptualization.

Declaration of competing interest

The authors declare that they have no competing financial interests or personal relationships that have influenced the work reported in this paper.

Data availability

The complete dataset and R code scripts to elaborate on corrections and analysis are found in supplementary materials for transparency

Acknowledgments

This work was inspired by Dr. Sarah Pederzani and colleagues' research on silver phosphate methods (see references therein), we thank Dr. Pederzani (University of La Laguna, Spain) for help and insights

during the early stages of the method development. We thank Dr. Jessica L. Blois (UC Merced, USA), Dr. Stephen C. Hart (UC Merced, USA), and Dr. Jürgen Kriwet (University of Vienna, Austria) from Larocca Conte's dissertation committee for their valuable insights during the experimental design stage. This work would not be possible without Dr. Asmeret Asefaw Berhe, Dr. Teamrat A. Ghezzehei, Dr. David Rice, and Dr. Peggy O'Day (UC Merced, USA) who let us use their facilities during the data collection stage, even during the limited lab access periods of COVID-19. Finally, we are grateful to Dr. Robert G. Dundas (California State University, Fresno, USA) and Dr. Scott Rufolo (Canadian Museum of Nature, Canada) for loaning the fossil bone and shark samples, respectively. We thank three anonymous reviewers and Dr. Julie Griffin for their constructive reviews that improved the manuscript through the peer review process. The project analyses and GLC were supported by the NSF Award #1842049 to SLK.

Appendix A. Supplementary data

Supplementary data to this article can be found online at https://doi.org/10.1016/j.chemgeo.2024.122000.

References

Abderrahim, B., Mohamed, H., Abla, F., 2016. Study on thermal desalination effect on the solids' precipitation variation. Desalin. Water Treat. 57, 5926–5931. https://doi.org/10.1080/19443994.2015.1038733.

Al Sekhaneh, W., Akkam, Y.H., Kamel, G., Drabee, A., Popp, J., 2021. Investigation of ancient teeth using Raman spectroscopy and synchrotron radiation Fourier-transform infrared (SR-μFTIR): mapping and novel method of dating. Dig. J. Nanomater. Biostruct. 16, 713–724.

Andersohn, C., 1996. Phosphate cycles in energy crop systems with emphasis on the availability of different phosphate fractions in the soil. Plant Soil 184, 11–21. https://doi.org/10.1007/BF00029270.

Atwater, J.E., 2002. Complex dielectric permittivities of the Ag2O-Ag2CO3 system at microwave frequencies and temperatures between 22 °C and 189 °C. Appl. Phys. A Mater. Sci. Process. 75, 555–558. https://doi.org/10.1007/s003390201308.

Barnes, P.A., O'Connor, M.F., Stone, F.S., 1971. Reactivity of silver oxide in the absorption of carbon dioxide. J. Chem. Soc. A Inorganic, Phys. J. Chem. Soc. A Inorg. Phys. Theor. Chem. 3395–3398. https://doi.org/10.1039/J19710003395.

Biedermann, G., Sillén, L.G., Lindberg, B., Dodson, R.M., 1960. Studies on the hydrolysis of metal ions. Part 30. A critical survey of the solubility equilibria of Ag2O. Acta Chem. Scand. 14, 717–725. https://doi.org/10.3891/acta.chem.scand.14-0717.

Bio-Rad Laboratories, 2000. AG 1, AG MP-1, and AG 2 Strong Anion Exchange Resin Instruction Manual Table of Contents.

Botella, H., Valenzuela-Ríos, J.I., Martínez-Perez, C., 2009. Tooth replacement rates in early chondrichthyans: a qualitative approach. Lethaia 42, 365–376. https://doi.org/10.1111/j.1502-3931.2009.00152.x.

Bowes, J.H., Elliott, R.G., Moss, J.A., 1955. The composition of collagen and acid-soluble collagen of bovine skin. Biochem. J. 61, 143–150. https://doi.org/10.1042/bj0610143.

Charlot, G., 1969. Les réactions chimiques en solution; l'analyse qualitative minérale, 6th ed. Masson et Cie, Paris.

Colman, A.S., 2002. The Oxygen Isotope Composition of Dissolved Inorganic Phosphate and the Marine Phosphorus Cycle. Yale University.

Colman, A.S., Blake, R.E., Karl, D.M., Fogel, M.L., Turekian, K.K., 2005. Marine phosphate oxygen isotopes and organic matter remineralization in the oceans. Proc. Natl. Acad. Sci. U. S. A. 102, 13023–13028. https://doi.org/10.1073/PNAS.0506455102/SUPPL_FILE/06455SUPPTEXT.PDF.

Cox, J.D., Head, A.J., 1962. Solubility of carbon dioxide in hydrofluoric acid solutions: "Standard state" correction for the combustion calorimetry of organo-fluorine compounds. Trans. Faraday Soc. 58, 1839–1845. https://doi.org/10.1039/TF9625801839.

Crowley, B.E., Wheatley, P.V., 2014. To bleach or not to bleach? Comparing treatment methods for isolating biogenic carbonate. Chem. Geol. 381, 234–242. https://doi.org/10.1016/j.chemgeo.2014.05.006.

Crowson, R.A., Showers, W.J., Wright, E.K., Hoering, T.C., 1991. Preparation of phosphate samples for oxygen isotope analysis. Anal. Chem. 63, 2397–2400. https://doi.org/10.1021/ac00020a038.

Dettman, D.L., Kohn, M.J., Quade, J., Ryerson, F.J., Ojha, T.P., Hamidullah, S., 2001. Seasonal stable isotope evidence for a strong Asian monsoon throughout the past 10.7 m.y. Geology 29, 31–34. https://doi.org/10.1130/0091-7613(2001)?029<0031:SSIEFA>?2.0.CO.

Dorozhkin, S.V., 2009. Calcium orthophosphates in nature, biology and medicine. Materials (Basel). https://doi.org/10.3390/ma2020399.

Dupont, 2019a. Product Data Sheet AMBERLITE TM IRN78 OH Ion Exchange Resin.

Dupont, 2019b. AmberChromTM Fine Mesh Ion Exchange Resins Technical Manual For Fine Chemical and Pharmaceutical Column.

Enax, J., Prymak, O., Raabe, D., Epple, M., 2012. Structure, composition, and mechanical properties of shark teeth. J. Struct. Biol. 178, 290–299. https://doi.org/10.1016/j.jsb.2012.03.012.

Enax, J., Janus, A.M., Raabe, D., Epple, M., Fabritius, H.O., 2014. Ultrastructural organization and micromechanical properties of shark tooth enameloid. In: Acta Biomaterialia. Elsevier Ltd, pp. 3959–3968. https://doi.org/10.1016/j.actbio.2014.04.028.

Firsching, F.H., 1961. Precipitation of silver phosphate from homogeneous solution. Anal. Chem. 33, 873–874. https://doi.org/10.1021/ac60175a018.

Fourel, F., Martineau, F., Lécuyer, C., Kupka, H.J., Lange, L., Ojeimi, C., Seed, M., 2011. 18O/16O ratio measurements of inorganic and organic materials by elemental analysis-pyrolysis-isotope ratio mass spectrometry continuous-flow techniques. In: Rapid Communications in Mass Spectrometry. John Wiley and Sons Ltd, pp. 2691–2696. https://doi.org/10.1002/rcm.5056.

Fox-Dobbs, K., Stidham, T.A., Bowen, G.J., Emslie, S.D., Koch, P.L., 2006. Dietary controls on extinction versus survival among avian megafauna in the late Pleistocene. Geology 34, 685–688. https://doi.org/10.1130/G22571.1.

Fox-Dobbs, K., Dundas, R.G., Trayler, R.B., Holroyd, P.A., 2014. Paleoecological implications of new megafaunal 14C ages from the McKittrick tar seeps, California. J. Vertebr. Paleontol. 34, 220–223. https://doi.org/10.1080/02724634.2013.791694.

France, C.A.M., Giaccai, J.A., Doney, C.R., 2015. The effects of Paraloid B-72 and Butvar B-98 treatment and organic solvent removal on δ13C, δ15N, and δ18O values of collagen and hydroxyapatite in a modern bone. Am. J. Phys. Anthropol. 157, 330–338. https://doi.org/10.1002/ajpa.22697.

Fuller, B.T., Fahrni, S.M., Harris, J.M., Farrell, A.B., Coltrain, J.B., Gerhart, L.M., Ward, J. K., Taylor, R.E., Southon, J.R., 2014. Ultrafiltration for asphalt removal from bone collagen for radiocarbon dating and isotopic analysis of Pleistocene fauna at the tar pits of Rancho La Brea, Los Angeles, California. Quat. Geochronol. 22, 85–98. https://doi.org/10.1016/j.quageo.2014.03.002.

Garvie-Lok, S.J., Varney, T.L., Katzenberg, M.A., 2004. Preparation of bone carbonate for stable isotope analysis: the effects of treatment time and acid concentration. J. Archaeol. Sci. 31, 763–776. https://doi.org/10.1016/j.jas.2003.10.014.

Goldhammer, T., Brüchert, V., Ferdelman, T.G., Zabel, M., 2010. Microbial sequestration of phosphorus in anoxic upwelling sediments. Nat. Geosci. 38 (3), 557–561. https://doi.org/10.1038/ngeo913.

Goldhammer, T., Max, T., Brunner, B., Einsiedl, F., Zabel, M., 2011. Marine sediment pore-water profiles of phosphate δ18O using a refined micro-extraction. Limnol. Oceanogr. Methods 9, 110–120. https://doi.org/10.4319/lom.2011.9.110.

Griffin, J.M., Montañez, I.P., Matthews, J.A., Bates, S., Lyons, T.W., 2015. A refined protocol for δ18OPO4 analysis of conodont bioapatite. Chem. Geol. 417, 11–20. https://doi.org/10.1016/j.chemgeo.2015.08.025.

Grimes, V., Pellegrini, M., 2013. A comparison of pretreatment methods for the analysis of phosphate oxygen isotope ratios in bioapatite. Rapid Commun. Mass Spectrom. 27, 375–390. https://doi.org/10.1002/rcm.6463.

Grunenwald, A., Keyser, C., Sautereau, A.M., Crubézy, E., Ludes, B., Drouet, C., 2014. Novel contribution on the diagenetic physicochemical features of bone and teeth minerals, as substrates for ancient DNA typing. Anal. Bioanal. Chem. 406, 4691–4704. https://doi.org/10.1007/s00216-014-7863-z.

Gu, L.-S., Huang, X.-Q., Griffin, B., Bergeron, B.R., Pashley, D.H., Niu, L.-N., Tay, F.R., 2017. Primum non nocere – the effects of sodium hypochlorite on dentin as used in endodontics. Acta Biomater. 61, 144–156. https://doi.org/10.1016/j.actbio.2017.08.008.

Guo, D., Wang, J., Silva, G., Gao, S., 2013. Reactivity and mechanism study of CO2 with amino acids as carbon capture solvents. Energy Fuel 27, 3898–3904. https://doi.org/10.1021/EF400413R/SUPPL_FILE/EF400413R_SI_001.PDF.

Haq, S., Rehman, W., Waseem, M., Meynen, V., Awan, S.U., Saeed, S., Iqbal, N., 2018. Fabrication of pure and moxifloxacin functionalized silver oxide nanoparticles for photocatalytic and antimicrobial activity. J. Photochem. Photobiol. B Biol. 186, 116–124. https://doi.org/10.1016/j.jphotobiol.2018.07.011.

Karnes, M.E., Chan, R.L., Kuntz, J.P., Griffiths, M.L., Shimada, K., Becker, M.A., Maisch, H.M., Eagle, R.A., Brenner-Coltrain, J., Miller, S., Kim, S.L., 2024. Enigmatic carbonate isotope values in shark teeth: evidence for environmental and dietary controls. Palaeogeogr. Palaeoclimatol. Palaeoecol. 635, 111943 https://doi.org/10.1016/J.PALAEO.2023.111943.

Kim, S.L., Eberle, J.J., Bell, D.M., Fox, D.A., Padilla, A., 2014. Evidence from shark teeth for a brackish Arctic Ocean in the Eocene greenhouse. Geology 42, 695–698. https://doi.org/10.1130/G35675.1.

Kim, S.L., Zeichner, S.S., Colman, A.S., Scher, H.D., Kriwet, J., Mörs, T., Huber, M., 2020. Probing the ecology and climate of the Eocene Southern Ocean with Sand Tiger Sharks Striatolamia macrota. Paleoceanogr. Paleoclimatol. 35 https://doi.org/10.1029/2020PA003997 e2020PA003997.

Kirsanow, K., Makarewicz, C., Tuross, N., 2008. Stable oxygen (δ18O) and hydrogen (δD) isotopes in ovicaprid dentinal collagen record seasonal variation. J. Archaeol. Sci. 35, 3159–3167. https://doi.org/10.1016/J.JAS.2008.06.025.

Koch, P.L., Tuross, N., Fogel, M.L., 1997. The effects of sample treatment and diagenesis on the isotopic integrity of carbonate in biogenic hydroxylapatite. J. Archaeol. Sci. 24, 417–429. https://doi.org/10.1006/jasc.1996.0126.

Köck, E.M., Kogler, M., Bielz, T., Klötzer, B., Penner, S., 2013. In situ FT-IR spectroscopic study of CO2 and CO adsorption on Y2O3, ZrO2, and yttria-stabilized ZrO 2. J. Phys. Chem. C 117, 17666–17673. https://doi.org/10.1021/JP405625X/SUPPL_FILE/JP405625X_SI_001.PDF.

Kocsis, L., Gheerbrant, E., Mouflih, M., Cappetta, H., Yans, J., Amaghzaz, M., 2014. Comprehensive stable isotope investigation of marine biogenic apatite from the late Cretaceous-early Eocene phosphate series of Morocco. Palaeogeogr. Palaeoclimatol. Palaeoecol. 394, 74–88. https://doi.org/10.1016/j.palaeo.2013.11.002.

Kohn, M.J., Cerling, T.E., 2003. Stable Isotope Compositions of Biological Apatite. Rev. Mineral. Geochem. 48, 455–488.
Kohn, M.J., Schoeninger, M.J., Barker, W.W., 1999. Altered states: Effects of diagenesis on fossil tooth chemistry. Geochim. Cosmochim. Acta 63, 2737–2747. https://doi.org/10.1016/S0016-7037(99)00208-2.
Kolodny, Y., Luz, B., Navon, O., 1983. Oxygen isotope variations in phosphate of biogenic apatites, I. Fish bone apatite-rechecking the rules of the game. Earth Planet. Sci. Lett. 64, 398–404. https://doi.org/10.1016/0012-821X(83)90100-0.
Kornexl, B.E., Gehre, M., Höfling, R., Werner, R.A., 1999. On-line δ18O measurement of organic and inorganic substances. Rapid Commun. Mass Spectrom. 13, 1685–1693. https://doi.org/10.1002/(sici)1097-0231(19990830)13:16<1685::aid-rcm699>3.0.co;2-9.
Kumar, H., Rani, R., 2013. Structural characterization of silver nanoparticles synthesized by micro emulsion route. Int. J. Eng. Innov. Technol. 3, 344–348.
L'vov, B.V., 1999. Kinetics and mechanism of thermal decomposition of silver oxide. Thermochim. Acta 333, 13–19. https://doi.org/10.1016/S0040-6031(99)00085-4.
Lapworth, D.J., Surridge, B., Williams, P.J., Heaton, T.H.E., Gooddy, D.C., 2014. Method for analysing phosphate 18O/16O ratios for waters with high C:P ratios. Br. Geol. Surv. 16.
Lebon, M., Reiche, I., Gallet, X., Bellot-Gurlet, L., Zazzo, A., 2016. Rapid quantification of bone collagen content by ATR-FTIR spectroscopy. Radiocarbon 58, 131–145. https://doi.org/10.1017/RDC.2015.11.
Lécuyer, C., 2004. Oxygen isotope analysis of phosphate. Handb. Stable Isot. Anal. Tech. 482–496 https://doi.org/10.1016/B978-044451114-0/50024-7.
Lécuyer, C., Grandjean, P., O'Neil, J.R., Cappetta, H., Martineau, F., 1993. Thermal excursions in the ocean at the Cretaceous-Tertiary boundary (northern Morocco): δ18O record of phosphatic fish debris. Palaeogeogr. Palaeoclimatol. Palaeoecol. 105, 235–243. https://doi.org/10.1016/0031-0182(93)90085-W.
Lécuyer, C., Grandjean, P., Barrat, J.A., Nolvak, J., Emig, C., Paris, F., Robardet, M., 1998. δ18O and REE contents of phosphatic brachiopods: a comparison between modern and lower Paleozoic populations. Geochim. Cosmochim. Acta 62, 2429–2436. https://doi.org/10.1016/S0016-7037(98)00170-7.
Lécuyer, C., Fourel, F., Martineau, F., Amiot, R., Bernard, A., Daux, V., Escarguel, G., Morrison, J., 2007. High-precision determination of 18O/16O ratios of silver phosphate by EA-pyrolysis-IRMS continuous flow technique. J. Mass Spectrom. 42, 36–41. https://doi.org/10.1002/jms.1130.
Lee-Thorp, J., 2002. Two decades of progress towards understanding fossilization processes and isotopic signals in calcified tissue minerals. Archaeometry 44, 435–446. https://doi.org/10.1111/1475-4754.t01-1-00076.
Lee-Thorp, J.A., van der Merwe, N.J., 1991. Aspects of the chemistry of modern and fossil biological apatites. J. Archaeol. Sci. 18, 343–354. https://doi.org/10.1016/0305-4403(91)90070-6.
LeGeros, R.Z., 1981. Apatites in biological systems. Prog. Cryst. Growth Charact. 4, 1–45. https://doi.org/10.1016/0146-3535(81)90046-0.
Leventouri, T., 2006. Synthetic and biological hydroxyapatites: crystal structure questions. Biomaterials 27, 3339–3342. https://doi.org/10.1016/j.biomaterials.2006.02.021.
Liu, H., Huang, K., 2016. Structural characteristics of extracted collagen from Tilapia (Oreochromis mossambicus) bone: effects of ethylenediaminetetraacetic acid solution and hydrochloric acid treatment. Int. J. Food Prop. 19, 63–75. https://doi.org/10.1080/10942912.2014.951939.
Lübke, A., Enax, J., Loza, K., Prymak, O., Gaengler, P., Fabritius, H.O., Raabe, D., Epple, M., 2015. Dental lessons from past to present: ultrastructure and composition of teeth from plesiosaurs, dinosaurs, extinct and recent sharks. RSC Adv. 5, 61612–61622. https://doi.org/10.1039/c5ra11560d.
Marending, M., Luder, H.U., Brunner, T.J., Knecht, S., Stark, W.J., Zehnder, M., 2007. Effect of sodium hypochlorite on human root dentine - mechanical, chemical and structural evaluation. Int. Endod. J. 40, 786–793. https://doi.org/10.1111/j.1365-2591.2007.01287.x.
McMahon, K.W., Hamady, L.L., Thorrold, S.R., 2013. A review of ecogeochemistry approaches to estimating movements of marine animals. Limnol. Oceanogr. https://doi.org/10.4319/lo.2013.58.2.0697.
Merck KGaA, 2018. Ultrafree ® -MC and -CL Centrifugal Filter Devices with Microporous Membranes.
Mine, A.H., Waldeck, A., Olack, G., Hoerner, M.E., Alex, S., Colman, A.S., 2017. Microprecipitation and δ18O analysis of phosphate for paleoclimate and biogeochemistry research. Chem. Geol. 460, 1–14. https://doi.org/10.1016/j.chemgeo.2017.03.032.
Murphy, J., Riley, J.P., 1962. A modified single solution method for natural determination of phosphate in natural waters. Anal. Chim. Acta 27, 13–19.
Newsome, S.D., Clementz, M.T., Koch, P.L., 2010. Using stable isotope biogeochemistry to study marine mammal ecology. Mar. Mamm. Sci. 26, 509–572. https://doi.org/10.1111/j.1748-7692.2009.00354.x.
Ni, G., Dou, H., Li, Z., Zhu, C., Sun, G., Hu, X., Wang, G., Liu, Y., Wang, Z., 2022. Study on the combustion characteristics of bituminous coal modified by typical inorganic acids. Energy 261, 125214. https://doi.org/10.1016/j.energy.2022.125214.
Nishiyama, N., Suzuki, K., Nagatsuka, A., Yokota, I., Nemoto, K., 2003. Dissociation states of collagen functional groups and their effects on the priming efficacy of HEMA bonded to collagen. J. Dent. Res. 82, 257–261. https://doi.org/10.1177/154405910308200403.
Oje, A.I., Ogwu, A.A., Mirzaeian, M., Tsendzughul, N., Oje, A.M., 2019. Pseudo-capacitance of silver oxide thin film electrodes in ionic liquid for electrochemical energy applications. J. Sci. Adv. Mater. Dev. 4, 213–222. https://doi.org/10.1016/j.jsamd.2019.04.003.
O'Neil, J.R., Roe, L.J., Reinhard, E., Blake, R.E., 1994. A rapid and precise method of oxygen isotope analysis of biogenic phosphate. Isr. J. Earth Sci. 43, 203–212.
Pearson, P.N., Foster, G.L., Wade, B.S., 2009. Atmospheric carbon dioxide through the Eocene-Oligocene climate transition. Nature 461, 1110–1113. https://doi.org/10.1038/nature08447.
Pederzani, S., Britton, K., 2019. Oxygen isotopes in bioarchaeology: principles and applications, challenges and opportunities. Earth-Sci. Rev. https://doi.org/10.1016/j.earscirev.2018.11.005.
Pederzani, S., Snoeck, C., Wacker, U., Britton, K., 2020. Anion exchange resin and slow precipitation preclude the need for pretreatments in silver phosphate preparation for oxygen isotope analysis of bioapatites. Chem. Geol. 534, 119455 https://doi.org/10.1016/j.chemgeo.2019.119455.
Pellegrini, M., Snoeck, C., 2016. Comparing bioapatite carbonate pre-treatments for isotopic measurements: Part 2 - Impact on carbon and oxygen isotope compositions. Chem. Geol. 420, 88–96. https://doi.org/10.1016/j.chemgeo.2015.10.038.
Pucéat, E., Joachimski, M.M., Bouilloux, A., Monna, F., Bonin, A., Motreuil, S., Morinière, P., Hénard, S., Mourin, J., Dera, G., Quesne, D., 2010. Revised phosphate-water fractionation equation reassessing paleotemperatures derived from biogenic apatite. Earth Planet. Sci. Lett. 298, 135–142. https://doi.org/10.1016/j.epsl.2010.07.034.
Quinton, P.C., Leslie, S.A., Herrmann, A.D., MacLeod, K.G., 2016. Effects of extraction protocols on the oxygen isotope composition of conodont elements. Chem. Geol. 431, 36–43. https://doi.org/10.1016/j.chemgeo.2016.03.023.
Rahman, M.M., Alam, M.M., Hussain, M.M., Asiri, A.M., Zayed, M.E.M., 2018. Hydrothermally prepared Ag2O/CuO nanomaterial for an efficient chemical sensor development for environmental remediation. Environ. Nanotech. Monit. Manag. 10, 1–9. https://doi.org/10.1016/j.enmm.2018.04.001.
Ramírez-Bommer, C., Gulabivala, K., Ng, Y.L., Young, A., 2018. Estimated depth of apatite and collagen degradation in human dentine by sequential exposure to sodium hypochlorite and EDTA: a quantitative FTIR study. Int. Endod. J. 51, 469–478. https://doi.org/10.1111/iej.12864.
Rashmi, B.N., Harlapur, S.F., Avinash, B., Ravikumar, C.R., Nagaswarupa, H.P., Anil Kumar, M.R., Gurushantha, K., Santosh, M.S., 2020. Facile green synthesis of silver oxide nanoparticles and their electrochemical, photocatalytic and biological studies. Inorg. Chem. Commun. 111, 107580 https://doi.org/10.1016/j.inoche.2019.107580.
Royer, A., Lécuyer, C., Montuire, S., Escarguel, G., Fourel, F., Mann, A., Maureille, B., 2013. Late Pleistocene (MIS 3-4) climate inferred from micromammal communities and δ18O of rodents from Les Pradelles, France. Quat. Res. (U.S.) 80, 113–124. https://doi.org/10.1016/j.yqres.2013.03.007.
RStudio Team, 2021. RStudio: Integrated Development for R.
Sasagawa, I., 1999. Fine structure of dental epithelial cells and the enameloid during the enameloid formation stages in an elasmobranch, *Heterodontus japonicus*. Anat. Embryol. (Berl.) 200, 477–486. https://doi.org/10.1007/s004290050296.
Schwarcz, H.P., Schoeninger, M.J., 1991. Stable isotope analyses in human nutritional ecology. Am. J. Phys. Anthropol. 34, 283–321. https://doi.org/10.1002/ajpa.1330340613.
Shabaga, B.M., Gough, H., Fayek, M., Hoppa, R.D., 2018. A simplified silver phosphate extraction method for oxygen isotope analysis of bioapatite. Rapid Commun. Mass Spectrom. 32, 1237–1242. https://doi.org/10.1002/rcm.8149.
Shemesh, A., Kolodny, Y., Luz, B., 1983. Oxygen isotope variations in phosphate of biogenic apatites, II. Phosphorite rocks. Earth Planet. Sci. Lett. 64, 405–416. https://doi.org/10.1016/0012-821X(83)90101-2.
Shimabukuro, M., Hayashi, K., Kishida, R., Tsuchiya, A., Ishikawa, K., 2022. No-observed-effect level of silver phosphate in carbonate apatite artificial bone on initial bone regeneration. ACS Infect. Dis. 8, 159–169. https://doi.org/10.1021/acsinfecdis.1c00480.
Sibbesen, E., 1978. An investigation of the anion-exchange resin method for soil phosphate extraction. Plant Soil 50, 305–321. https://doi.org/10.1007/BF02107180.
Siddiqui, M.R.H., Adil, S.F., Assal, M.E., Ali, R., Al-Warthan, A., 2013. Synthesis and characterization of silver oxide and silver chloride nanoparticles with high thermal stability. Asian J. Chem. 25, 3405–3409. https://doi.org/10.14233/ajchem.2013.13874.
Slager, T.L., Lindgren, B.J., Mallmann, A.J., Greenler, R.G., 1972. Infrared spectra of the oxides and carbonates of silver. J. Phys. Chem. 76, 940–943. https://doi.org/10.1021/j100650a029.
Snoeck, C., Pellegrini, M., 2015. Comparing bioapatite carbonate pre-treatments for isotopic measurements: Part 1-Impact on structure and chemical composition. Chem. Geol. 417, 394–403. https://doi.org/10.1016/j.chemgeo.2015.10.004.
Stephan, E., 2000. Oxygen isotope analysis of animal bone phosphate: method refinement, influence of consolidants, and reconstruction of palaeotemperatures for Holocene sites. J. Archaeol. Sci. 27, 523–535. https://doi.org/10.1006/jasc.1999.0480.
Sun, Y., Wiedenbeck, M., Joachimski, M.M., Beier, C., Kemner, F., Weinzierl, C., 2016. Chemical and oxygen isotope composition of gem-quality apatites: Implications for oxygen isotope reference materials for secondary ion mass spectrometry (SIMS). Chem. Geol. 440, 164–178. https://doi.org/10.1016/j.chemgeo.2016.07.013.
Suthanthiraraj, S.A., Sarumathi, R., 2012. XRD and FTIR studies on a new solid electrolyte system containing Ag 3PO4 and SbI3. AIP Conf. Proc. 1447, 1005–1006. https://doi.org/10.1063/1.4710345.
Suwanprateeb, J., Thammarakcharoen, F., Wasoontararat, K., Chokevivat, W., Phanphiriya, P., 2012. Preparation and characterization of nanosized silver phosphate loaded hydroxyapatite by single step co-conversion process. Mater. Sci. Eng. C 32, 2122–2128. https://doi.org/10.1016/j.msec.2012.05.051.
Tabor, R.F., Chan, D.Y.C., Grieser, F., Dagastine, R.R., 2011. Anomalous stability of carbon dioxide in pH-controlled bubble coalescence. Angew. Chem. 123, 3516–3518. https://doi.org/10.1002/ange.201006552.

Trayler, R.B., Landa, P.V., Kim, S.L., 2023. Evaluating the efficacy of collagen isolation using stable isotope analysis and infrared spectroscopy. J. Archaeol. Sci. 151, 105727 https://doi.org/10.1016/j.jas.2023.105727.

Trivedi, K.M., Tallapragada, R.M., Branton, A., Trivedi, D., Nayak, G., Jana, S., Latiyal, O., 2015. The potential impact of biofield energy treatment on the physical and thermal properties of silver oxide powder. Int. J. Biomed. Sci. Eng. 3, 62. https://doi.org/10.11648/j.ijbse.20150305.11.

Tsutaya, T., Yoneda, M., 2015. Reconstruction of breastfeeding and weaning practices using stable isotope and trace element analyses: a review. Am. J. Phys. Anthropol. 156, 2–21. https://doi.org/10.1002/AJPA.22657.

Tütken, T., Vennemann, T.W., Janz, H., Heizmann, E.P.J., 2006. Palaeoenvironment and palaeoclimate of the Middle Miocene lake in the Steinheim basin, SW Germany: a reconstruction from C, O, and Sr isotopes of fossil remains. Palaeogeogr. Palaeoclimatol. Palaeoecol. 241, 457–491. https://doi.org/10.1016/j.palaeo.2006.04.007.

Vennemann, T.W., Hegner, E., 1998. Oxygen, strontium, and neodymium isotope composition of fossil shark teeth as a proxy for the palaeoceanography and palaeoclimatology of the Miocene northern Alpine Paratethys. Palaeogeogr. Palaeoclimatol. Palaeoecol. 142, 107–121. https://doi.org/10.1016/S0031-0182(98)00062-5.

Vennemann, T.W., Hegner, E., Cliff, G., Benz, G.W., 2001. Isotopic composition of recent shark teeth as a proxy for environmental conditions. Geochim. Cosmochim. Acta 65, 1583–1599. https://doi.org/10.1016/S0016-7037(00)00629-3.

Vennemann, T.W., Hegner, E., Cliff, G., Benz, G.W., 2001. Isotopic composition of recent shark teeth as a proxy for environmental conditions. Geochim. Cosmochim. Acta 65, 1583–1599. https://doi.org/10.1016/S0016-7037(00)00629-3.

Vennemann, T.W., Fricke, H.C., O'Neil, J.R., Colman, A., 2002. Oxygen isotope analysis of phosphates: a comparison of techniques for for analysis of Ag3PO4. Chem. Geol. 185, 321–336. https://doi.org/10.1016/S0009-2541(01)00413-2.

Wiedemann-Bidlack, F.B., Colman, A.S., Fogel, M.L., 2008. Phosphate oxygen isotope analysis on microsamples of bioapatite: removal of organic contamination and minimization of sample size. Rapid Commun. Mass Spectrom. 22, 1457–1466. https://doi.org/10.1002/rcm.3553.

Xue, Y., Hu, Z., Wang, C., Xiao, Y., 2019. Evaluation of dissolved organic carbon released from aged asphalt binder in aqueous solution. Constr. Build. Mater. 218, 465–476. https://doi.org/10.1016/j.conbuildmat.2019.05.060.

Yürüm, Y., Dror, Y., Levy, M., 1985. Effect of acid dissolution on the mineral matrix and organic matter of Zefa EFE oil shale. Fuel Process. Technol. 11, 71–86. https://doi.org/10.1016/0378-3820(85)90017-7.

Zacke, A., Voigt, S., Joachimski, M.M., Gale, A.S., Ward, D.J., Tütken, T., 2009. Surface-water freshening and high-latitude river discharge in the Eocene North Sea. J. Geol. Soc. Lond. 166, 969–980. https://doi.org/10.1144/0016-76492008-068.

Zazzo, A., Lécuyer, C., Mariotti, A., 2004. Experimentally-controlled carbon and oxygen isotope exchange between bioapatites and water under inorganic and microbially-mediated conditions. Geochim. Cosmochim. Acta 68, 1–12. https://doi.org/10.1016/S0016-7037(03)00278-3.

Zhang, L., Li, Z., Yang, Y., Zhou, Y., Kong, B., Li, J., Si, L., 2016. Effect of acid treatment on the characteristics and structures of high-sulfur bituminous coal. Fuel 184, 418–429. https://doi.org/10.1016/j.fuel.2016.07.002.

Zhang, M., Hao, P., Dong, S., Li, Y., Yuan, G., 2020. Asphalt binder micro-characterization and testing approaches: a review. Meas. J. Int. Meas. Confed. 151, 107255 https://doi.org/10.1016/j.measurement.2019.107255.

Zhang, X., Hoff, I., Saba, R.G., 2021. Response and deterioration mechanism of bitumen under acid rain erosion. Materials (Basel) 14.

Žigaite, Ž., Whitehouse, M., 2014. Stable oxygen isotopes of dental biomineral: Differentiation at the intra- and inter-tissue level of modern shark teeth. GFF 136, 337–340. https://doi.org/10.1080/11035897.2013.878747.